QUANTUM ENTANGLEMENT PRODUCING AND PRECISION MEASUREMENT WITH SPINOR BECS

by

Zhen Zhang

A dissertation submitted in partial fulfillment
of the requirements for the degree of
Doctor of Philosophy
(Physics)
in the University of Michigan
2015

Doctoral Committee:

Professor Luming Duan, Chair
Associate Professor Hui Deng
Professor Georg A. Raithel
Professor Duncan G. Steel
Assistant Professor Kai Sun

To my parents and my husband.

ACKNOWLEDGMENTS

I am greatly indebted to my adviser, Professor Luming Duan, for mentoring me over the last six years. He is a wise professor with sharp insights and broad knowledge and also a kind and supportive supervisor. He offered me a lot help and advise both in my research and for my career. It has been my great honor working with him during my doctoral study.

I would also like to thank my undergraduate research adviser Professor Mailin Liang , Professor Wusheng Dai and Professor Mi Xie at Tianjin University, China, for guiding me into the world of physics research and offering initial scientific training. I am also grateful to all the other professors who gave me advice and help imparted their knowledge and enthusiasm through classroom teaching or otherwise during the ten years of undergraduate and graduate study.

I also benefited tremendously from my group mates and visitors. In particular, Zhexuan Gong who gave me warm welcome and help when I joined the group; Yang-Hao Chan who taught me cold atom physics in the very beginning of my research; Jiang-Min Zhang shared with me a lot of knowledge and experience both in research and in personal life; Dong-Ling Deng and Sheng-Tao Wang discussed with me on many problems. There were also previous group members and visitors whose stay had brief overlap with mine or I met in other occasions I would like to thank, Shi-Liang Zhu, Yue Wu, Emily Lichko. I am also very grateful to the whole graduate class of 2009 for being so nice and kind. I would also like to thank the fellow Asian students, Lei Zhang for helpful discussion and his enthusiastic research attitude, Bo Zhang for many airport rides, Jiaming Yu and Chunpeng Wang for being supportive friends Lulu Liu, Hang Chi, Ying Zhou, Anbo Chen

, Zhichen Zhao and Langechuan Liu for help in one way or another. There are a lot of other friends I could not mention due to space limitation.

Finally I wish to thank my family. I thank my parents for respecting my choices. I thank my husband for emotional support and encouragement during my hard time.

TABLE OF CONTENTS

LIST OF FIGURES

LIST OF APPENDICES

ABSTRACT

A lot of progress has been made for the control of single particle nowadays and various precise manipulation of small scaled quantum systems have also been demonstrated. The development of quantum technology makes the task to built large scaled practical devices possible. In a large scaled quantum system the extent of entanglement in the quantum state is a key point for both pratical use and theoretical research. Preparation and utilizing of a strongly entangled quantum states are of strong interest and in great need.

In this dissertation we focused on some quantum states with strong entanglement and robustness to noise. We constructed a spinor BEC Hamiltonian which has already been realized in experiment with several different kinds of atom and proposed a adiabatic passage method to produce the maximum entangled Dicke state.

We also analyzed the entanglement behavior of the Dicke state under various noises and demonstrate its application in high precision measurement experiment. We introduce a new class of quantum many-particle entangled states, called the Dicke squeezed (or DS) states, which can be used to improve the precision in quantum metrology beyond the standard quantum limit. We show that the enhancement in measurement precision is characterized by a single experimentally detectable parameter, called the Dicke squeezing ξ_D, which also bounds the entanglement depth for this class of states. The measurement precision approaches the ultimate Heisenberg limit as ξ_D attains the minimum in an ideal Dicke state. Compared with other entangled states, we show that

the Dicke squeezed states are more robust to decoherence and give better measurement precision under typical experimental noise.

In addition, we explore other choices of precision measurement with spin squeezed states. Spin squeezed states have strong manybody entanglement and are good candidates to be used in quantum metrology. A robust squeezing parameter is proposed to characterize the experimental phase measurement precision for spin squeezed states. The behavior of this parameter under various experimental noises is compared with other parameters in literature and it is shown to have better performance.

Finally we present a scalable implementation scheme for the recently proposed concept of boson sampling, which holds the promise of outperforming classical computers in the near future. Boson sampling solves a classically intractable problem by sampling from a probability distribution given by matrix permanents. We propose a scalable implementation of Boson sampling using local transverse phonon modes of trapped ions to encode the bosons. The proposed scheme allows deterministic preparation and high-efficiency readout of the Bosons in the Fock states and universal mode mixing. With the state-of-the-art trapped ion technology, it is feasible to realize Boson sampling with tens of Bosons by this scheme, which would outperform the most powerful classical computers and constitute an effective disproof of the famous extended Church-Turing thesis. A complete recipe is provided and the technical requirements are discussed.

CHAPTER I

Introduction

1.1 Motivation

The Turing machine invented by Alan Turing in 1936 was a milestone for computer science, as it helps computer scientists understand the limits of mechanical computation, which is essential the same for all kinds of physical devices. The situation changed in 1980s when the idea of quantum Turing machine were proposed by David Deutsch. The using of quantum algorithms greatly improved the computation power of computers. The combination of computation theory and quantum cold atomic physics lead to the prosperousness of the interdisciplinary field of quantum information processing and quantum computation.

The experimental realization of Bose-Einstein condensates in 1995, which was predicted by Einstein in 1925, offers robust and versatile systems for probing the fundamental problems and finding applications in these interdisciplinary fields, and the study of ultracold Bose gases has been one of the most active areas in contemporary physics. Bose gases with internal degrees of freedom serve as a great candidate for the implementation of quantum computation and quantum information processing, with their excellent capability to generate quantum entanglement, which is a key

ingredient of the realization of quantum computers and many quantum information protocols.

The searching for an appropriate quantum state with strong entanglement and a good experimental system are of great interest nowadays. Quantum gates with a small number of qubits have been analyzed and experimentally produced, quantum states with a large number of particles and strong entanglement properties are studied and various realization candidates have been proposed, such as atomic BECs, trapped ions and photonic systems. This dissertation focuses on problems in the preparation and analysis of entangled quantum states, precision improvement in quantum metrology and the implementation of a non-traditional paradigm of quantum computing–boson sampling.

1.2 Background

Before we dive into detailed discussions of the major topics, we briefly review the physical platform considered , i.e. spinor BECs. Spinor BEC systems have been utilized for a wide range of purposes from quantum computation. Useful entangled states that can be realized using spinor BEC are also introduced.

1.2.1 Spinor BECs

For Bose-Einstein condensate (BEC) trapped in a magnetic field which chooses only the spin ground state, their spin degrees of freedom are frozen. However, the spinor BEC, which is a BEC with internal spin degrees of freedom, is confined using optical trap and thereby all spin substates are simultaneously condensed. The vector spin field can exhibit more interesting phenomena. In this section we deduce the Hamiltonian for spinor BECs in an optical trap with both spin interaction and external potential.

The noninteracting part of the Hamiltonian consists of the kinetic part, trapping potential and the effect in magnetic field with the following form:

$$\hat{H}_0 = \sum_{m,n=-f}^{f} \int d\mathbf{r}\, \hat{\psi}_m^\dagger [-\frac{\hbar^2\nabla^2}{2M} + U(\mathbf{r}) - p(f_z)_{mn} + q(f_z^2)_{mn}]\hat{\psi}_n$$

where $\hat{\psi}_m(\mathbf{r})$ denote the bosonic field operators for spin-f atoms with the spin index $m = -f, -(f-1), ...f-1, f$. M is the mass of the atom, and $U(\mathbf{r})$ represent the external trapping potential. The magnetic effect is evaluated by the linear Zeeman coefficient $p = -g\mu_B B$ and the quadratic Zeeman coefficient $q = \frac{(g\mu_B B)^2}{\Delta E_{hf}}$, where g is the Landé g factor, μ_B is the Bohr magneton, B is the external magnetic field and ΔE_{hf} is the hyperfine energy splitting. f_z is the z component of the spin matrices which is a diagonal matrix with the form of $(f_z)_{mn} = m\delta_{mn}$ and f_z^2 matix has the form of $(f_z^2)_{mn} = m^2\delta_{mn}$ correspondingly.

In the interacting part of the Hamiltonian only binary interaction is considered as we assume that the system is dilute. Since the total spin $\mathscr{F}$ is conserved in the binary collision, the interaction Hamiltonian has the form of

$$\hat{V} = \sum_{\mathscr{F}=0,2,...,2f} \hat{V}^{(\mathscr{F})}$$

Only terms with even $\mathscr{F}$ exist as the result of symmetry consideration. In the single particle representation, interaction Hamiltonian takes the form of

$$\hat{V}^{(\mathscr{F})} = \frac{1}{2}\int d\mathbf{r} \int d\mathbf{r}' \frac{4\pi\hbar^2}{M} a_{\mathscr{F}} \delta(\mathbf{r}-\mathbf{r}') \sum_{\mathscr{M}=-\mathscr{F}}^{\mathscr{F}} \hat{A}^\dagger_{\mathscr{F}\mathscr{M}}(\mathbf{r},\mathbf{r}')\hat{A}_{\mathscr{F}\mathscr{M}}(\mathbf{r},\mathbf{r}')$$

with $a_{\mathscr{F}}$ as the s-wave scattering length and operator [1]

$$\hat{A}_{\mathscr{F}\mathscr{M}}(\mathbf{r},\mathbf{r}') = \sum_{m_1,m_2=-f}^{f} \langle \mathscr{F},\mathscr{M}|f,m_1;f,m_2\rangle \hat{\psi}_{m_1}(\mathbf{r})\hat{\psi}_{m_2}(\mathbf{r})$$

$\langle \mathscr{F},\mathscr{M}|f,m_1;f,m_2\rangle$ is the Clebsch-Gordan coefficients for total spin $\mathscr{F}$ and z spin component with the value of $\mathscr{M}$.

In the case of spin-1 particles, with some derivations the interaction part of the Hamiltonian can also expressed as

$$\hat{V} = \frac{1}{2}\int d\mathbf{r}[c_0' : \hat{n}^2(\mathbf{r}) : + c_1' : \hat{F}^2(\mathbf{r}) :]$$

with the particle density operator

$$\hat{n}(\mathbf{r}) = \sum_{m=-f}^{f} \hat{\psi}_m^{\dagger}(\mathbf{r})\hat{\psi}_m(\mathbf{r})$$

and the spin operator

$$\hat{F}(\mathbf{r}) = \sum_{m,n=-f}^{f} (f_\mu)_{mn}\hat{\psi}_m^{\dagger}(\mathbf{r})\hat{\psi}_n(\mathbf{r}),$$

and the interaction coefficients are $c_0' = 4\pi\hbar^2(a_0+2a_2)/3M$ and $c_1' = 4\pi\hbar^2(a_2-a_0)/3M$.

1.2.2 Precision Measurement and Ramsey Interferometry

Precision measurement plays an important role for scientific and technological applications, and one of the most important application of the systems with high measurement precision is atomic

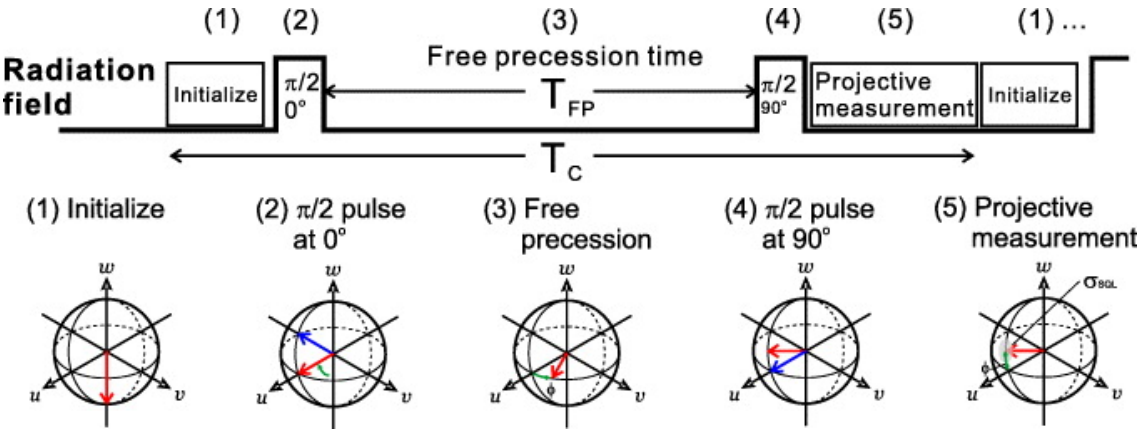

Figure 1.2.1: Illustration of Ramsey interferometry process. The x, y, z axis are denoted by u, v, and w. This figure is taken from [4].

clock. The most commonly used interferometry scheme for atomic clock is Ramsey interferometry and we will introduce the method below.

Ramsey interferometry, also known as Ramsey-Bordé interferometry, is a form of atom interferometry that uses the phenomenon of magnetic resonance to measure transition frequencies of atoms. It was developed in 1949 by Norman Ramsey [2]. The system used is a two-level atom with transition frequency ω_0 and a local oscillator (LO) with frequency ω, and the frequency offset is $\delta\omega = \omega - \omega_0$. The atomic transition frequency is decided by measuring the relative phase difference $\delta\phi = \delta\omega T$ in a free evolution period with time length T.

We will review the Ramsey method using the Bloch representation [3]. The five-step process is illustrated in Fig. 1.2.1 For the first step the two-level atom with two states $|\uparrow\rangle$ and $|\downarrow\rangle$ in the z direction is prepared in the $|\downarrow\rangle$ state, then a microwave $\pi/2$ pulse is performed on the atom and will result in a 90^0 rotation around the y axis. After the rotation the atom evolves with the interaction with the LO for a time period of T and the accumulated phase difference is $\delta\phi = \delta\omega T$ around the z axis. After the free evolution another microwave $\pi/2$ pulse is added for a 90^0 rotation around x axis. The final stage is the measurement of the atom in the $|\uparrow\rangle$ or $|\downarrow\rangle$ state. To decide the phase difference, multiple measurements will be performed on a large number of atoms simultaneously.

The measurement precision of the phase difference $\delta\phi$ is determined by the stability of the atomic state. Decoherence will happen in realistic experiment and there will be unavoidable noises. With long coherence time the evolution time T can be maximized. There are proposals to use entangled atoms for the purpose of long coherence time and lower noise [5–7]. For N particles in unentangled states, the phase precision is constrained by the standard quantum limit of $1/\sqrt{N}$ and by using entangled states the precision can reach the Heisenberg limit of $1/N$ under noiseless condition and the effect of various noises will be discussed in later chapters.

1.2.3 Spin Squeezed States

Among all entangled states, spin squeezed states have a lot interesting and unique properties. They can be used in quantum metrology for high precision measurement where Heisenberg limit might be reached.

According to Heisenberg's uncertainty relation, fluctuations of angular momentum in different directions are limited by the inequation

$$\Delta J_x \cdot \Delta J_y \geq |\langle J_z \rangle|/2$$

If we want to suppress the uncertainty of spin in the x or y direction to be lower than the standard limit of $\sqrt{|\langle J_z \rangle|/2}$, then the spin fluctuation in another direction will be increased without violating the Heisenberg's uncertainty relation. It is natural to define spin squeezed states as states with $\Delta^2 J_i < |\langle J_j \rangle|/2$ for $i \neq j$.

To characterize the squeezing behavior of a state, Wineland [7] proposed a spin squeezing parameter

$$\xi = \frac{\sqrt{2J}\Delta J_x}{|\langle J_z \rangle|}$$

for systems of N two-level atoms with J as the total spin. $\xi < 1$ indicates that spin in the x direction is squeezed and the smaller ΔJ_x can be reached the stronger squeezing we have.

This squeezing parameter does not only characterize the squeezing level of a state. It can also work as an entanglement witness as spin squeezed states are entangled quantum states.

To get the maximum squeezing we will check how small ξ can be. Sorensen and Molmer show that for fixed total spin $J = \frac{N}{2}$ and total spin in the z direction J_z, the minimum variance $Var(J_x)$ can be calculated numerically. The analysis for integer spins and for half-integer spins are different so they are discussed separately.

For integer spins, the state with minimum $Var(J_x)$ for a given $\langle J_z \rangle$ also has $\langle J_x \rangle = \langle J_y \rangle = 0$. So that minimizing $Var(J_x)$ is equivalent to minimizing $\langle J_x^2 \rangle$. Thereby an easy way to find the state with minimum ξ for fixed $\langle J_z \rangle$ is to find the minimum of $\mu \langle J_z \rangle + \langle J_x^2 \rangle$ with μ as the Lagrange multiplier.

For half-integer spins, this method does not work as states with minimum $Var(J_x)$ are not states with minimum $\langle J_x^2 \rangle$. However we can still find the most squeezed state by minimizing $\mu \langle J_z \rangle + Var\langle J_x^2 \rangle$.

The maximum squeezed states are strongly entangled and are hard to prepare in real experiment, and there are a lot proposals to generate states with strong squeezing in history. The most popular method to generate squeezing in a quantum state is to perform a unitary transformation $U(t) = \exp[-iHt]$ generated by a Hamiltonian H of a special form on the coherent spin state (CSS) . The CSS of spin-half atoms is a pure state with every qubit with a wave function of

$$|\theta, \phi\rangle = cos\frac{\theta}{2}|\uparrow\rangle + e^{i\phi} sin\frac{\theta}{2}|\downarrow\rangle$$

where $|\uparrow\rangle$ and $|\downarrow\rangle$ are the up and down eigenstate for S_z. As there is no correlation between atoms so the CSS is not spin squeezed.

As the transformation resulted by Hamiltonian linear in spin operators are only rotations, nonlinear Hamiltonians are needed to generate squeezing. The one-axis twisting (OAT) and two-axis countertwisting (TAT) approaches using different Hamiltonian setting are introduced in [8] .

For OAT, the initial CSS is picked to be $|\frac{\pi}{2},0\rangle$ and the Hamiltonian is chosen as $H=\chi J_z^2$. With the evolution time properly chosen, the final state will be squeezed with $\Delta J_{min}^2 \approx \frac{1}{2}(\frac{J}{3})^{1/3}$.

There are both experimental OAT squeezing scheme realized for a large number of atoms [9] [10] and theoretical proposals [11] for improvement, and it is proven that the noise-to-signal ratio is reduced to an amount proportional to $N^{-2/3}$ for s system of N atoms.

For TAT, the initial CSS $|0,\phi\rangle$ is squeezed using Hamiltonian $H=\chi(J_+^2-J_-^2)$, with $J_+=\frac{J_x+iJ_y}{2}$ and $J_-=\frac{J_x-iJ_y}{2i}$. With this squeezing the minimum variance ΔJ_{min}^2 that can be reached is as low as $\frac{1}{2}$ while strict experimental condition is required.

1.2.4 Trapped Ions

Trapped ion system can be isolated from the environment by proper trapping and brought nearly to rest using laser cooling. In the mean while their internal states can be well manipulated by optical fields. This makes them ideal candidates for quantum computation and quantum information processing.

The initial guess to form a three dimensional trap for charged atomic ions is to make use of electric fields. The electric potential has the form of $\Phi(x,y,z)=\alpha x^2+\beta y^2+\gamma z^2$ and the coefficients must satisfy the requirement that $\alpha+\beta+\gamma=0$, which is the result of the zero charge Maxwell equation $\nabla^2\Phi=0$. From this constraint we have the conclusion that there exists no real three dimensional electric trapping potential for ions as at least one of the three coeffients must be negetive. The ideal

of Paul trap was proposed by Wolfgang Paul in 1950s to solve this problem. Instead of just using electrostatic traps, an electric field oscillating at radio frequency (RF) is applied. In the $x-y$ plane radio frequency electric fields are employed to generate an effective trap and in the z direction a pure static trapping potential is used. This makes an overall potential of

$$\Phi(x,y,z) = \alpha\cos(\Omega t)(x^2-y^2) - \frac{\gamma}{2}(x^2+y^2) + \gamma z^2$$

With a proper oscillation frequency Ω in the radio frequency regime and integrating out the high frequency dynamics, this potential results in a trap potential of

$$\Phi(x,y,z) = \alpha'(x^2+y^2) + \gamma z^2$$

where $\alpha \gg \alpha' > 0$ and $\gamma > 0$. Thereby a time independent harmonic trap is realized. The typical value for $\alpha'$and γ are on the order of 1-10 MHZ.

Atoms with two valence electrons are used in trapped ion systems. Two internal levels are identified after loosing one electron, and these two levels can serve as the qubit states. The behavior of the qubits can be controlled by using laser beams with appropriate frequency. With laser beams focused on one single ion single qubit gate operation can be realized, and the proposal of the controlled-NOT gate in 1995 by Ignacio Cirac and Peter Zoller [12] and its implementation in 2003 [13] made the universal quantum computing possible.

1.3 Outline of Dissertation

To orient the readers, we provide a brief outline of the contents of this dissertation.

Chapters II, III and IV focus on the spinor BEC systems. Chapter II deals with the generalization

of massive entanglement in a spinor Bose-Einstein condensate from an initial product state through adiabatic sweep of magnetic field across a quantum phase transition induced by competition between the spin-dependent collision interaction and the quadratic Zeeman effect. The generated many-body entanglement is characterized by the experimentally measurable entanglement depth in the proximity of the Dicke state. We show that the scheme is robust to practical noise and experimental imperfection and under realistic conditions it is possible to generate genuine entanglement for hundreds of atoms.

Chapter III introduce a new class of quantum many-particle entangled states, called the Dicke squeezed (or DS) states, which can be used to improve the precision in quantum metrology beyond the standard quantum limit. We show that the enhancement in measurement precision is characterized by a single experimentally detectable parameter, called the Dicke squeezing ξ_D, which also bounds the entanglement depth for this class of states. The measurement precision approaches the ultimate Heisenberg limit as ξ_D attains the minimum in an ideal Dicke state. Compared with other entangled states, we show that the Dicke squeezed states are more robust to decoherence and give better measurement precision under typical experimental noise.

In Chapter IV we proposed a robust squeezing parameter to characterize the experimental phase measurement precision for spin squeezed states. The behavior of this parameter under various experimental noises is compared with other parameters in the history and it is shown to have better performance.

Chapter V discusses the implementation of a boson sampler in the trapped ion platform. A scalable implementation of Boson sampling using local transverse phonon modes of trapped ions to encode the Bosons was proposed, which allows deterministic preparation and high-efficiency readout of the Bosons in the Fock states and universal mode mixing. With the state-of-the-art trapped ion technology, it is feasible to realize Boson sampling with tens of Bosons by this scheme, which would outperform the most powerful classical computers and constitute an effective disproof of

the famous extended Church-Turing thesis.

The last chapter will conclude the dissertation and discuss future directions for the topics covered.

CHAPTER II

Generation of Massive Entanglement in a Spinor Condensate

2.1 Background Information

Generation of massive entanglement, besides its interest for foundational research of quantum theory, is of great importance for applications in quantum information processing and precision measurements. Entanglement is a valuable resource that can be used to enhance the performance of quantum computation, the security of quantum communication, and the precision of quantum measurements. For these applications, it is desirable to get as many particles as possible into entangled states. However, entanglement is typically fragile and many-particle entangled states can be easily destroyed by decoherence due to inevitable coupling to the environment. As an experimental record, so far fourteen qubits carried by trapped ions have been successfully prepared into genuine entangled states [14]. Pushing up this number represents a challenging goal in the experimental frontier.

The Bose Einstein condensate of ultracold atoms is in a pure quantum mechanical state with strong collision interaction. In a spinor condensate [1, 15–17], the spin-dependent collision interaction can be used to produce spin squeezing [9, 10, 18–20], which is an indicator of many-particle entangle-

ment [21]. Spin squeezing has been demonstrated in condensates in recent experiments through spin-dependent collision dynamics [9, 10, 20, 22, 23]. A squeezed state is typically sensitive to noise and generation of substantial squeezing requires accurate control of experimental systems, which is typically challenging. In quantum information theory, the Dicke states are known to be relatively robust to noise and they have important applications for quantum metrology [24] and implementation of quantum information protocols [25]. For instance, the three-particle Dicke state, the so-called W state, has been proven to be the most robust entangled state under particle loss [26]. Because of their applications and nice noise properties, Dicke states represent an important class of many-body states that are pursued in physical implementation. For a few particles, Dicke states have been generated in several experimental systems [27, 28] .

2.2 Chapter Outline

In this chapter, we propose a robust method to generate massive entanglement in the proximity of many-particle Dicke states through control of adiabatic passage across a quantum phase transition in a spinor condensate. Using conservation of the magnetic quantum number, we show that sweep of the magnetic field across the polar-ferromagnetic phase transition provides a simple method to generate many-body entanglement in this mesoscopic system. The generated many-body entanglement can be characterized through the entanglement depth, which measures how many particles have been prepared into genuine entangled states [21, 29]. The entanglement depth can be easily measured experimentally for this system through a criterion introduced in Ref. [30]. We quantitatively analyze the entanglement production through the entanglement depth and show that the scheme is robust under noise and experimental imperfection. The scheme works for both the ferromagnetic (such as ^{87}Rb) and the anti-ferromagnetic (such as ^{23}Na) condensates. For the anti-ferromagnetic case, we use adiabatic quantum phase transition in the highest eigenstate of the

Hamiltonian instead of its ground state.

2.3 System and Hamiltonian Description

The system under consideration is a ferromagnetic (or anti-ferromagnetic) spin-1 Bose Einstein condensate under an external magnetic field, which has been realized with ^{87}Rb (or ^{23}Na) atoms in an optical trap [1]. The spin-independent collision rate of a spinor condensate is typically much larger than the spin-dependent one. In this case, to describe the ground state of the spinor condensate in a spin-independent optical trap, it is good approximation to assume that different spin components of the condensate take the same spatial wave function $\phi(\mathbf{r})$. This is the well-known single mode approximation [1, 17], and under this approximation we have the atomic field operator $\hat{\psi}_m \approx \hat{a}_m \phi(\mathbf{r}), (m = 1, 0, -1)$, where a_m is the annihilation operator for corresponding spin mode. We assume the spinor condensate has a fixed total particle number N as in experiments and neglect the terms in the Hamiltonian that are constant under this condition. The relevant part of the Hamiltonian for a spinor condensate then takes the form [1, 17]

$$H = c_1 \frac{\mathbf{L}^2}{N} + \sum_{m=-1}^{1} (qm^2 - pm) a_m^\dagger a_m \tag{2.3.1}$$

where c_1 denotes the spin-dependent collision energy, p (q) corresponds respectively to the linear (quadratic) Zeeman energy shift, and $\mathbf{L}_\mu \equiv \sum_{m,n} a_m^\dagger (f_\mu)_{mn} a_n$ is the spin-1 angular momentum operator. The symbol f_μ ($\mu = x, y, z$) denotes μ-component of the spin-1 matrix, and $(f_\mu)_{mn}$ is the corresponding (m, n) matrix element. The derivation of this Hamiltonian is in the supplement A. We have $c_1 < 0$ ($c_1 > 0$) for ^{87}Rb (^{23}Na), which corresponds to ferromagnetic (anti-ferromagnetic) interaction, respectively. The linear Zeeman term $\sum_{m=-1}^{1} pm a_m^\dagger a_m = pL_z$ typical dominates in the Hamiltonian H. However, this term commutes with all the other terms in the Hamiltonian. If we start with an initial state that is an eigenstate of L_z, the linear Zeeman term has no effect and thus

can be neglected. In this paper, we consider an initial state with all the atoms prepared to the level $|F=1,m=0\rangle$ through optical pumping, which is an eigenstate of L_z. The system remains in this eigenstate with magnetization $L_z=0$, and the effective spin Hamiltonian becomes

$$H = c_1 \frac{\mathbf{L}^2}{N} - q a_0^\dagger a_0. \tag{2.3.2}$$

The ratio q/c_1 is the only tunable parameter in this Hamiltonian, and depending on its value, the Hamiltonian has different phases resulting from competition between the quadratic Zeeman effect and the spin-dependent collision interaction.

2.4 Ground State Structure

We first consider the ferromagnetic case with $c_1 < 0$. For the initial state, we tune up the magnetic field to make the quadratic Zeeman coefficient $q \gg |c_1|$. In this limit, the second term $-qa_0^\dagger a_0$ dominates in the Hamiltonian H. The ground state of the Hamiltonian is given by an eigenstate of $a_0^\dagger a_0$ with the maximum eigenvalue N. This ground state can be prepared by putting all the atoms to the Zeeman level $|F=1,m=0\rangle$ through optical pumping. Then we slowly ramp down the magnetic field to zero. From the adiabatic theorem, the system remains in the ground state of the Hamiltonian H and the final state is the lowest-energy state of $H_F = c_1\mathbf{L}^2/N$, which is the Dicke state $|L=N,L_z=0\rangle$ that maximizes $\mathbf{L}^2$ with the eigenvalue $L(L+1)$. The Dicke state $|L=N,L_z=0\rangle$ is a massively entangled state of all the particles.

2.5 Adiabatic Evolution Analysis

The above simple argument illustrates the possibility to generate massive entanglement through an adiabatic passage. To turn this possibility into reality, however, there are several key issues we need to analyze carefully. First, we need to know what is the requirement of the sweeping speed of the parameter q to maintain an adiabatic passage. In particular, this adiabatic passage goes through a quantum phase transition where the energy gap approaches zero in the thermodynamical limit. So the evolution cannot be fully adiabatic for a large system. It is important to know how the energy gap scales with the particle number N for this mesoscopic system. Second, due to the non-adiabatic correction and other inevitable noise in a real experimental system, the final state is never a pure state and quite different from its ideal form $|L = N, L_z = 0\rangle$. For a many-body system with a large number of particles, the state fidelity is always close to zero with presence of just small noise. So we need to analyze whether we can still generate and confirm genuine many-particle entanglement under realistic experimental conditions.

To analyze the entanglement behavior, first we quantitatively calculate the phase transition points during this adiabatic passage and analyze how the energy gap scales with the particle number N. The mean-field phase diagram for the Hamiltonian (2.3.1) is well known [1]. However, in typical mean field calculations one fixes the parameters p, q to obtain the ground state of the Hamiltonian (2.3.1), and this ground state in general has varying magnetization $\langle L_z \rangle$. For our proposed adiabatic passage, we should fix $\langle L_z \rangle = 0$ and find the ground state of the Hamiltonian (2.3.2) instead of (2.3.1) as the linear Zeeman term is irrelevant.

We perform exact numerical many-body calculation in the Hilbert space with $\langle L_z \rangle = 0$ to find the ground state of the Hamiltonian (2.3.2) and draw the condensate fraction in the the Zeeman level $|F = 1, m = 0\rangle$, N_0/N with $N_0 \equiv \left\langle a_0^\dagger a_0 \right\rangle$, in Fig. 2.5.1 as we ramp down the parameter q. Control of the magnetic field can only sweep the parameter q from the positive side to zero. Further sweep

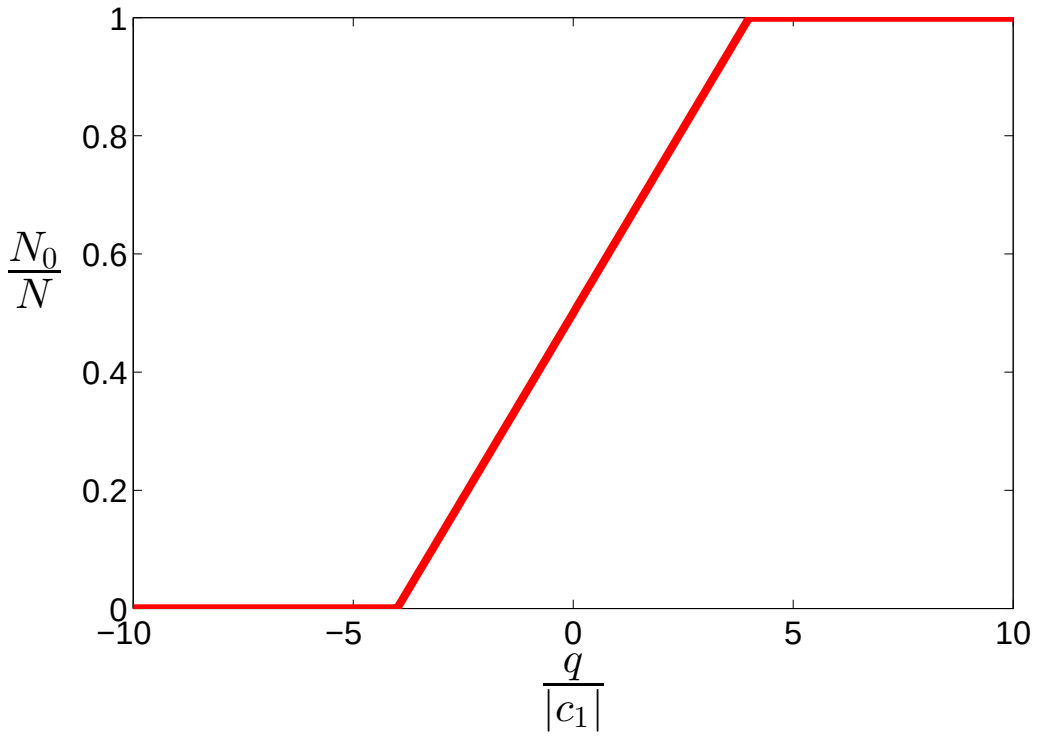

Figure 2.5.1: The order parameter $\langle N_0/N \rangle$ shown as a function of the quadratic Zeeman coefficient q in units of $|c_1|$ for the total atom number $N = 10^5$. Two second-order phase transitions take place at $q/|c_1| = \pm 4$.

of q to the negative side can be obtained through ac-Stack effect induced by a microwave field coupling the hyperfine levels $|F = 1\rangle$ and $|F = 2\rangle$, as demonstrated in experiments [31, 32].

The curve in Fig. 2.5.1 shows two second-order phase transitions at the positions $q/|c_1| = \pm 4$, where the condensate fraction N_0/N drop first from 1 to a positive number r $(0 < r < 1)$ and then to 0. The transition point at $q/|c_1| = 4$ agrees with the mean field prediction, however, there is a significant discrepancy for the transition at $q/|c_1| = -4$. Mean field calculation under a fixed parameter $p = 0$ predicts a transition at $q/|c_1| = 0$, where the magnetization $\langle L_z \rangle$ abruptly changes [1]. For the adiabatic passage considered here, due to the conservation of L_z the transition at $q/|c_1| = 0$ is postponed to the point $q/|c_1| = -4$.

Besides prediction of the phase transition points, the exact many-body calculation can show evo-

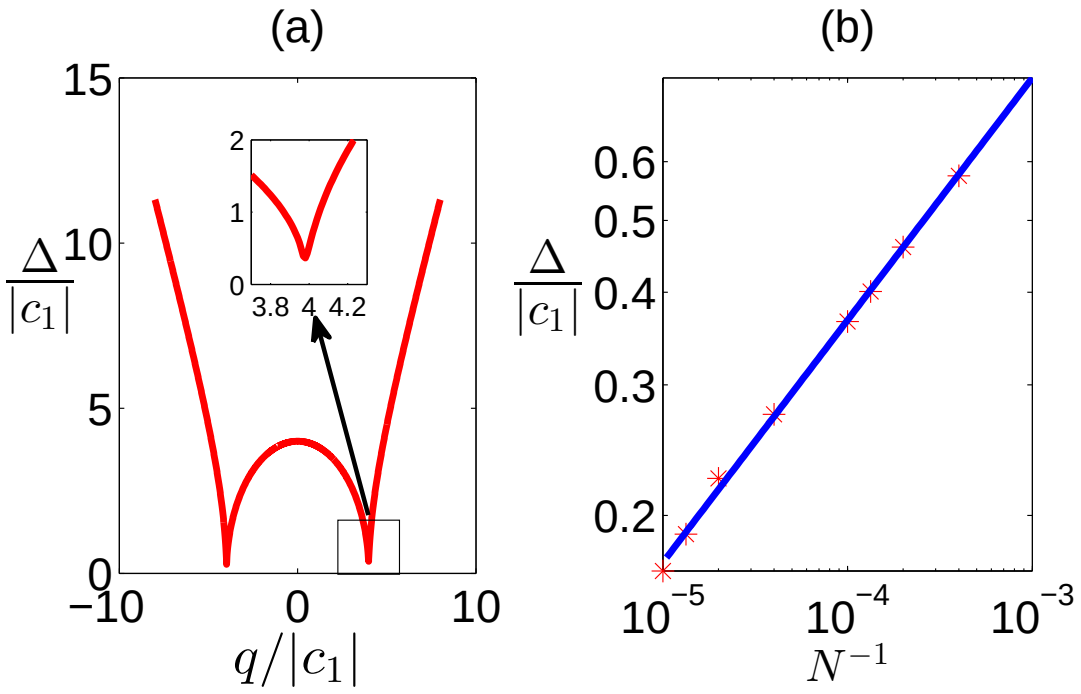

Figure 2.5.2: (a) The energy gap Δ in units of $|c_1|$ shown as a function of $q/|c_1|$ with the total particle number $N = 10^4$. (b) The stars show the scaling of the energy gap $\Delta/|c_1|$ at the phase transition point with the particle number N in the log-log plot. The solid line is a linear fit to the data points with $\Delta = 7.4N^{-1/3}$.

lution of entanglement for the ground state and scaling of the energy gap with the particle number N at the phase transition points. The scaling of the energy gap is important as it shows the relevant time scale to maintain the adiabatic passage. In Fig. 2.5.2(a), we show the energy gap Δ (defined as the energy difference between the ground state and the first excited state) in units of $|c_1|$ as a function of $q/|c_1|$ for $N = 10^4$ particles. The gap attains the minimum at the phase transition points and is symmetric with respect to the transitions at $q/|c_1| = \pm 4$. In Fig. 2.5.2(b), we show how the energy gap at the phase transition point scales with the particle number N. In the $\log - \log$ plot, the points are on a straight line, which can be well fit with the polynomial scaling $\Delta = 7.4N^{-1/3}$. The energy gap decreases slowly with increase of the particle number N, which suggests it is possible to maintain an adiabatic passage for typical experimental systems with $N \sim 10^5$.

2.6 Entanglement Generation

With this understanding, we now turn to our main task in this chapter to characterize entanglement generation with this adiabatic passage. For this purpose, we need to have a quantity to measure entanglement in the proximity of the Dicke state and this measure should be accessible to experimental detection.

Due to non-adiabatic corrections and inevitable noise in real experiments, we cannot assume that the system is in a pure state and the entanglement measure should work for any mixed states. Many-body entanglement can be characterized in different ways, and a convenient measure is the so-called entanglement depth which measures how many particles in an N-particle system have been prepared into genuine entangled states given an arbitrary mixed state of the system [21,29,30].

A quantity to measure the entanglement depth for N spin-$1/2$ particles has been provided in Ref. [30] based on measurements of the collective spin operators. It is straightforward to generalize this quantity to the case of N spin-1 particles. For N spin-1 particles, the collective spin operator is defined by $L = \sum_{i=1}^{N} l_i$, where l_i denotes the individual spin-1 operator. In terms of the bosonic mode operators, the collective spin operator has the standard decomposition

$$\mathbf{L}_\mu = \sum_{m,n} a_m^\dagger (f_\mu)_{mn} a_n \, (\mu = x,y,z;\, m,n = 0,\pm 1)$$

To characterize entanglement in the proximity of the Dicke state $|L = N, L_z = 0\rangle$, we measure the quantity

$$\xi = \frac{\langle L_x^2 \rangle + \langle L_y^2 \rangle}{N(1 + 4\langle (\Delta L_z^2) \rangle)} \tag{2.6.1}$$

If $\xi > m$, from the arguments that lead to theorem 1 of Ref. [30] we conclude that the system has at least genuine m-particle entanglement (i.e., the entanglement depth is bounded by m from below). For the ideal Dicke state $|L = N, L_z = 0\rangle$, one can easily verify that $\xi = N + 1 > N$, so all

the N particles are in a genuine entangled state. The final state of real experiments is in general a complicated mixed state which is impossible to be read out for many-particle systems. The power of the measure in Eq. (2.6.1) is that it gives an experimentally convenient way to bound the entanglement depth in this case through simple detection of the collective spin operators even though the system state remains unknown.

Now we show how the entanglement measure defined in Eq. (2.6.1) evolves when we adiabatically sweep the parameter q in the Hamiltonian (4.2.2). We ramp down the parameter q linearly from $q = 6|c_1|$ to 0 with a constant speed, starting from the initial product state with all the particles in the level $|F = 1, m = 0\rangle$.

The entanglement depth ξ in units of N (see supplemental material for calculation details) of the final state is shown in Fig. 2.6.1 (a) and 2.6.1 (b) as a function of the sweeping speed v (in units of $|c_1|^2$ by taking $\hbar = 1$) for $N = 10^3$ and $N = 10^4$, respectively. We can see that the entanglement depth increases abruptly from a few to the order of N when the speed v decreases below $|c_1|^2$. In the same figure, we also show the excitation probability of the final state (the probability to be not in the ground state).

For a small number of particles, the excitation probability typically correlates with the entanglement depth, and they jump roughly around the same value of the sweeping speed. However, for a large number of particles (e.g., $N \geq 10^4$), we can have the entanglement depth of the order of N while the excitation probability is near the unity as shown in Fig. 2.6.1 (b). This indicates that the entanglement in the proximity of the Dicke state is quite robust. Even when the sweep is not fully adiabatic and most of the atoms are excited to the low-lying excited states (meaning that the state fidelity decrease to almost zero), we can still have the entanglement depth close to N (meaning all the particles are still genuinely entangled).

As the energy gap Δ at the phase transition point decreases with the atom number N, one expects that the required sweeping time T to get substantial entanglement increases with N. However, this

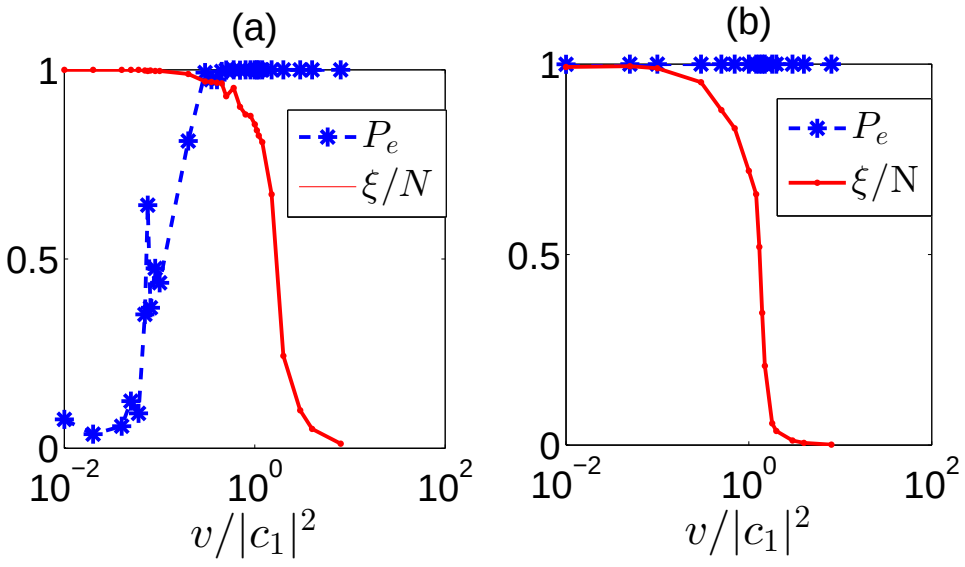

Figure 2.6.1: The normalized entanglement depth ξ/N (solid lines) and the excitation probability P_e (star points) for the final state shown as functions of the sweeping speed v (in units of $|c_1|^2$) for the number of particles $N = 10^3$ (a) and $N = 10^4$ (b). The parameter q in the Hamiltonian (4) is ramped down linearly from $q = 6|c_1|$ to 0 at a constant speed v, starting from the initial product state with all the particles in the level $|m = 0\rangle$.

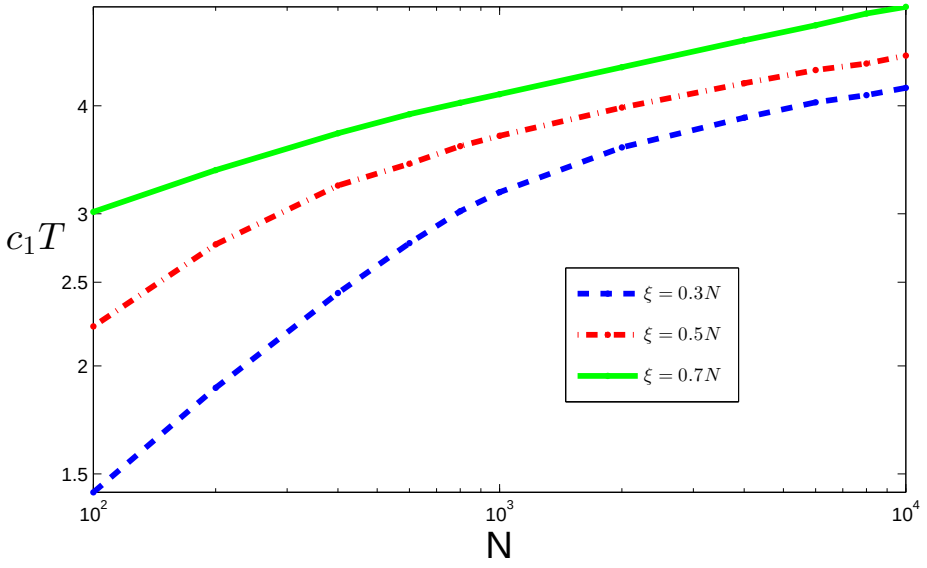

Figure 2.6.2: Scaling of the required sweeping time T (in units of $1/|c_1|$) with the particle number N as we fix the entanglement depth of the final state to be $0.3N$ (bottom curve), $0.5N$ (middle curve), and $0.7N$ (top curve), respectively.

increase is very slow. First, Δ decreases slowly with N by the scaling $\Delta \propto N^{-1/3}$ as shown in Fig. 2.5.2 (b). Second, for a large N even when $\Delta T < 1$ and a significant fraction of the atoms get excited during the sweep, we can still observe substantial entanglement as the entanglement depth of the low-lying excited states is still high as shown in Fig. 2.6.1 (b).

To see the the quantitative relation between the required sweeping time T and the particle number N, we fix the entanglement depth of the final state to be a significant number (e.g., with $\xi = 0.3N$, $0.5N$, or $0.7N$) and draw in Fig. 2.6.2 the scaling of T (in units of $1/|c_1|$) as a function of N. When $N \geq 10^3$, the curve of $|c_1|T$ is almost flat, increasing by a modest 20% when the atom number grows by an order of magnitude.

2.7 Choices of Experimental Platform

All the calculations above are done for the ferromagnetic case with $c_1 < 0$ by assuming an adiabatic sweep of the Hamiltonian (2.3.2) in its ground state. For the anti-ferromagnetic case with $c_1 > 0$ (such as ^{23}Na), we can perform an adiabatic sweep along the ground state of the Hamiltonian $-H$ (or the highest eigenstate of the Hamiltonian H in Eq. (2.3.2)). Then, all the calculations above equally apply to the anti-ferromagnetic case. The only difference is that initially the parameter q needs to be set to the negative side with $q = -6|c_1|$ when the atoms are prepared into the level $|m = 0\rangle$.

As mentioned before, q can be switched to both the positive and the negative sides, through ac-Stack shift from a π-polarized microwave field that couples the hyperfine levels $|F = 1\rangle$ and $|F = 2\rangle$ [31,32]. An advantage of using ^{23}Na instead of ^{87}Rb is that it is has a larger spin-dependent collision rate $|c_1|$ and thus allows a faster sweep of the parameter q. If we take the peak condensate density about $10^{14}cm^{-3}$, $c_1/\hbar$ is estimated to be about $-2\pi \times 7Hz$ for ^{87}Rb atoms and $2\pi \times 50Hz$ for ^{23}Na atoms.

2.8 Noise Robustness

Finally, we briefly discuss how the noise influence entanglement generation in this scheme. First, in the proximity of the Dicke state the entanglement depth measured through Eq. (2.6.1) is very robust to the dephasing noise (dephasing between the Zeeman levels caused by, e.g., a small fluctuating magnetic field).

As shown in Ref. [30], even with a dephasing error rate about 50% for each individual atom, the entanglement depth ξ remains about $N/2$, which is still large. The entanglement depth is more sensitive to the bit-flip error that increases $\langle \Delta L_z^2 \rangle$ in Eq. (2.6.1), which can be caused by imperfect preparation of the initial state, atom loss during the adiabatic sweep, linear Zeeman term in the Hamiltonian or imperfection in the final measurement of the collective spin operators.

The detection error can be corrected through simple data processing using the method proposed in Ref. [33] as long as its error rate has been calibrated.

The initial state $|F=1, m=0\rangle$ can be prepared efficiently through optical pumping and remaining atoms in the $|F=1, m=\pm 1\rangle$ levels can be blown away through microwave coupling to the $|F=2\rangle$ levels that are unstable under atomic collisions.

The atomic loss should be small as the sweeping time T is assumed to be much shorter compared with the life time of the condensate. Only loss of atoms in the components $|F=1, m=\pm 1\rangle$ can increase the fluctuation $\langle \Delta L_z^2 \rangle$. Assume the loss rate is p during the sweep, the resultant $\langle \Delta L_z^2 \rangle$ is estimated by $\langle \Delta L_z^2 \rangle \sim Np(1-p)/6$. For a large number of atoms with $Np \gg 1$, the entanglement depth in Eq. (2.6.1) is then estimated by $\xi \sim 3/(2p)$. If we take p about 1%, it is possible to prepare a remarkable number of hundreds of atoms into genuine entangled states.

2.9 Chapter Summary

We propose a method to generate massive entanglement in a spinor Bose-Einstein condensate from an initial product state through adiabatic sweep of magnetic field across a quantum phase transition induced by competition between the spin-dependent collision interaction and the quadratic Zeeman effect. The generated many-body entanglement is characterized by the experimentally measurable entanglement depth in the proximity of the Dicke state. We show that the scheme is robust to practical noise and experimental imperfection and under realistic conditions it is possible to generate genuine entanglement for hundreds of atoms.

This chaper contains content that was published elsewhere [34] and is available at

http://journals.aps.org/prl/abstract/10.1103/PhysRevLett.111.180401.

CHAPTER III

Quantum Metrology with Dicke Squeezed States

3.1 Background Information

Precision measurement plays an important role for scientific and technological applications. In many circumstances, precision measurement can be reduced to detection of a small phase shift by use of optical or atomic interferometry [35–38]. The precision of the phase measurement improves with increase of the number of particles (photons or atoms) in the interferometer. For N particles in non-entangled (classical) states, the phase sensitivity $\Delta\theta$ is constrained by the standard quantum limit $\Delta\theta \sim 1/\sqrt{N}$ from the shot noise [35, 37, 38].

Schemes have been proposed to improve the measurement precision beyond the standard quantum limit by use of quantum entangled states [35–42]. Two classes of states are particularly important for this scenario: one is the GHZ state [39], or called the NOON state in the second quantization representation [41, 42]; and the other is the spin squeezed state [35, 37, 38], which may include the squeezed state of light as a special limit. A number of intriguing experiments have been reported to prepare these states and use them for quantum metrology [9, 10, 43–47]. These states are typically sensitive to decoherence and experimental noise [48, 49]. As a result, the number of particles that

one can prepare into the GHZ state, or the maximal spin squeezing that one can achieve, are both severely limited in experiments by noise.

In this chapter, we introduce a new class of many-particle entangled states for quantum metrology, which we name as the Dicke squeezed (DS) states. The DS states have the following interesting features:

(i) They represent a wide class of entangled states with possibly many different forms but can be characterized by a single parameter called the Dicke squeezing ξ_D with $\xi_D < 1$. The Dicke squeezing parameter ξ_D can be conveniently measured in experiments from detection of the collective spin operator of N particles. It provides the figure of merit for application of the DS states in quantum metrology in the following sense: for states with ξ_D, the phase sensitivity $\Delta\theta$ and the phase measurement precision $d\theta$ both improve from the standard quantum limit $1/\sqrt{N}$ to the new scaling $\sqrt{\xi_D/N}$. The phase shift can be read out through the Bayesian inference for the DS states. Under a fixed particle number N, the parameter ξ_D attains the minimum $1/(N+2)$ under the ideal Dicke state, and the phase sensitivity correspondingly approaches the Heisenberg limit $\Delta\theta \sim 1/N$, in agreement with the previous result on the Dicke state [24, 50].

(ii) The entanglement of the DS states can be also characterized by the squeezing parameter ξ_D. For a many-body system with a large particle number N, we would like to know how many particles among them have been prepared into genuinely entangled states. This number of particles with genuine entanglement is called the entanglement depth for this system [21, 30]. A criterion proved in Ref. [30] by one of us indicates that $\xi_D^{-1} - 2$ gives a lower bound of the entanglement depth for any DS states with the squeezing parameter ξ_D.

(iii) Compared with the GHZ state or the spin squeezed states, we show that the DS states characterized by ξ_D are much more robust to decoherence and experimental noise such as particle loss. Substantial Dicke squeezing ξ_D remains under a significant amount of noise under which spin squeezing would not be able to survive at all.

3.2 The Spin Squeezing Parameter

For a system of N particles, each of two internal states a, b (with effective spin-$1/2$), we can define a Pauli matrix $\vec{\sigma_i}$ for each particle i and the collective spin operator $\vec{J}$ as the summation $\vec{J} = \sum_i \vec{\sigma_i}/2$. Note that the components of $\vec{J}$ can be measured globally without the requirement of separate addressing of individual particles.

If the particles are indistinguishable like photons or ultracold bosonic atoms, we can use the number of particles n_a, n_b in each mode a, b to denote the states. In this notation (second quantization representation), the GHZ state of N spins $|aa\cdots a\rangle + |bb\cdots b\rangle$ (unnormalized) is represented by $|N0\rangle_{ab} + |0N\rangle_{ab}$, the so called NOON state [41, 42].

The collective spin operators can be expressed in term of the mode operators a, b using the Schwinger representation $J_z = (a^\dagger a - b^\dagger b)/2$, $J_x = (a^\dagger b + b^\dagger a)/2$, $J_y = (a^\dagger b - b^\dagger a)/2i$ [36].

A small phase shift θ can be measured through the Mach-Zehnder type of interferometer illustrated in Fig. 3.4.1 by inputting a state of two modes a, b and measuring the number difference of the output modes (the output J_z operator). The two beam splitters in the interferometer exchange the J_z and J_y operators and the phase shifter is represented by a unitary operator $e^{i\theta J_z}$ which transforms J_y to $\cos\theta J_y - \sin\theta J_x$. Assume the input state has mean $\left\langle \vec{J} \right\rangle = \langle J_x \rangle$ and minimum variance $\left\langle (\Delta J_y)^2 \right\rangle$ along the y-direction. By measuring $\langle J_y' \rangle = \cos\theta \langle J_y \rangle - \sin\theta \langle J_x \rangle \approx -\theta \langle J_x \rangle$, the phase sensitivity $\Delta\theta$ is characterized by $\sqrt{\left\langle (\Delta J_y)^2 \right\rangle} / \langle J_x \rangle$. This motivates definition of the spin squeezing parameter [37, 38]

$$\xi_S = \frac{N \left\langle (\Delta J_y)^2 \right\rangle}{\langle J_x \rangle^2} \tag{3.2.1}$$

as the figure of merit for precision measurement. The phase sensitivity is estimated by $\sqrt{\xi_S/N}$ for this measurement scheme. There are also other spin squeezing parameters proposed in the history [51].

3.3 The Dicke Squeezing Parameter

Not all states useful for quantum metrology can be characterized by the spin squeezing ξ_S. An example is the Dicke state $|N/2,N/2\rangle_{ab}$, which has been shown to give the Heisenberg limited phase sensitivity in [24]. However, for this state $\left\langle \vec{J} \right\rangle = 0$ in all the directions, and the spin squeezing ξ_S is not a good measure to characterize states of this kind with $\left\langle \vec{J} \right\rangle = 0$. To characterize a broad class of states that are useful for quantum metrology, we introduce the following Dicke squeezing parameter, defined as

$$\xi_D = \frac{N(\langle (\Delta J_z)^2 \rangle + \frac{1}{4})}{\langle J_x^2 + J_y^2 \rangle}. \tag{3.3.1}$$

One can easily check that $\xi_D = 1$ for the benchmark spin-coherent states. We call any states with $\xi_D < 1$ as the Dicke squeezed states and a major result of this paper is to show that such states are useful for quantum metrology where the phase sensitivity is improved from $\sqrt{1/N}$ for the benchmark spin coherent state to about $\sqrt{\xi_D/N}$ for the DS states.

The parameter ξ_D attains the minimum $1/(N+2)$ under the ideal Dicke state $|N/2,N/2\rangle_{ab}$, and the phase sensitivity $\sqrt{\xi_D/N}$ correspondingly approaches the Heisenberg limit $\sim 1/N$, in agreement with the result in [24, 50].

The Dicke squeezing parameter ξ_D also characterizes the entanglement depth E_d for many-particle systems. For an N-qubit system, the entanglement depth E_d measures how many qubits have been prepared into genuinely entangled states [21, 30]. A theorem proven in Ref. [30] shows that $\lceil \xi_D^{-1} \rceil - 2$, where $\lceil \xi_D^{-1} \rceil$ denotes the minimum integer no less than ξ_D^{-1}, gives a lower bound of the entanglement depth E_d. For the ideal Dicke state, $|N/2,N/2\rangle_{ab}$, $\xi_D^{-1} = N+2$ and its entanglement depth is N [30].

Note that the entanglement depth characterizes the particle (qubit) entanglement when we express the state $|N/2,N/2\rangle_{ab}$ in the first quantization representation [21, 30], where one can easily see all the N qubits are genuinely entangled, so its entanglement depth is N. This should not be confused

with the mode entanglement between the bosonic operators a and b, which is zero for the Dicke state $|N/2,N/2\rangle_{ab}$.

So the defined Dicke squeezing parameter ξ_D provides a figure-of-merit both for entanglement characterization and its application in quantum metrology, and this parameter can be conveniently measured in experiments through detection of the collective spin operator $\overrightarrow{J}$.

3.4 The Internal Phase Precision

To show that ξ_D is the figure-of-merit for quantum metrology, we use two complementary methods to verify that the phase measurement precision is improved to $\sqrt{\xi_D/N}$ for a variety of states of different forms.

First, in the Mach-Zehnder (MS) interferometer shown in Fig. 3.4.1 (a), the phase sensitivity is estimated by the intrinsic uncertainty $\Delta\theta$ of the relative phase operator defined between the two arms (modes $a_{\pm}$). We calculate this phase uncertainty and find that it scales as $\sqrt{\xi_D/N}$ for various input states with widely different ξ_D and N.

Second, we directly estimate the phase shift θ by the Bayesian inference through detection of the spin operator J_z, and find that the measurement precision, quantified by the variance $d\theta$ of the posterior phase distribution, is well estimated by $\beta\sqrt{\xi_D/N}$, where $\beta \approx 1.7$ is a dimensionless prefactor.

We perform numerical simulation of experiments with randomly chosen phase shift θ and find that the difference between the actual θ and the the measured value of θ obtained through the Bayesian inference is well bounded by the variance $d\theta$, so $d\theta$ is indeed a good measure of the measurement precision.

The Dicke state $|N/2,N/2\rangle_{ab}$ represents an ideal limit, and it is hard to obtain a perfect Dicke state

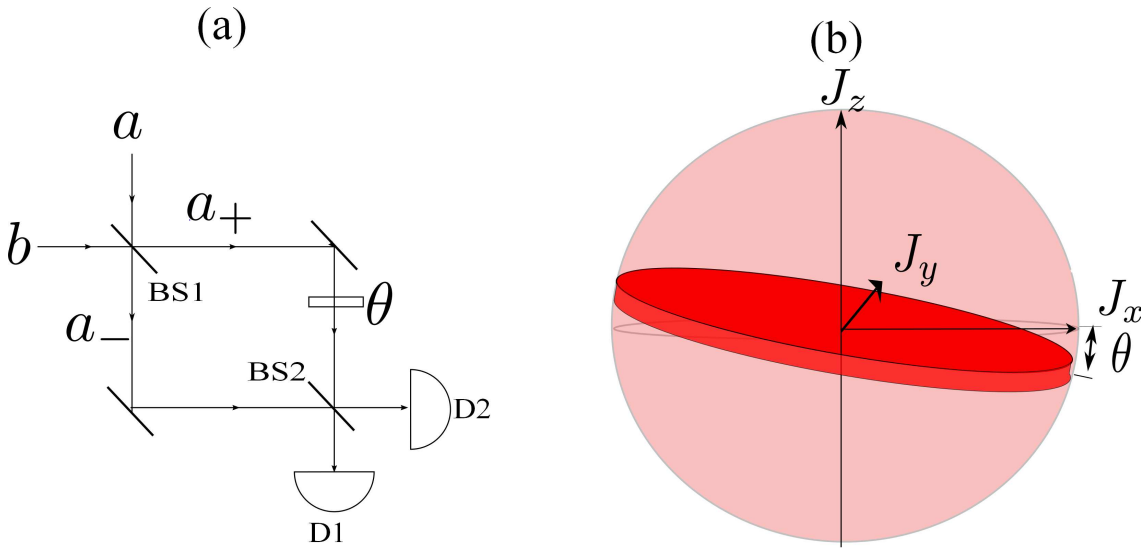

Figure 3.4.1: (a) The Mach-Zehnder (MZ) interferometer setup to measure the relative phase shift θ with input modes a, b in Dicke squeezed states. The detectors D1 and D2 measure the J_z operator by recording the particle number difference in the two output modes. (b) In the Bloch sphere for the collective spin operator $\vec{J}$, a measurement of the phase shift by the MZ interferometer is represented by rotation of a thin disk (its size in x, y, z directions corresponds to the variance of $\vec{J}$ under the Dicke squeezed state) by an angle θ.

in experiments in particular when the particle number N is large. Here, we consider two classes of more practical states as examples to show that ξ_D is the figure-of-merit for application in quantum metrology when the ideal Dicke state is distorted by unavoidable experimental imperfection.

For the first class, we consider pure states of the form $|\Psi(\sigma)\rangle_{ab} = \sum_{n=0}^{N} a_n(\sigma)|n, N-n\rangle$, where the total number of particles is fixed to be N but the number difference between the modes a, b follows a Gaussian distribution $a_n(\sigma) = exp\left\{\frac{-(n-\frac{N}{2})^2}{\sigma^2} + i\frac{\pi}{4}(n-\frac{N}{2})\right\}$ with different widths characterized by the parameter σ. The phase of $a_n(\sigma)$ is chosen for convenience so that the variance of the state is symmetric along the x, y axes.

For the second class, we consider mixed states $\rho_{ab}(\eta)$ which come from noise distortion of the Dicke state $|N/2, N/2\rangle_{ab}$ after a particle loss channel with varying loss rate η. To calculate $\rho_{ab}(\eta)$, we note that a loss channel with loss rate η can be conveniently modeled by the transformation $a = \sqrt{1-\eta}a_{in} + \sqrt{\eta}a_v$ and $b = \sqrt{1-\eta}b_{in} + \sqrt{\eta}b_v$, where a_{in}, b_{in} denote the annihilation operators of the input modes which are in the ideal Dicke state $|N/2, N/2\rangle = ((N/2)!)^{-1}(a_{in}^{\dagger}b_{in}^{\dagger})^{N/2}|0,0\rangle$ and a_v,b_v represent the corresponding vacuum modes. By substituting $a_{in}^{\dagger}, b_{in}^{\dagger}$ with $a^{\dagger}, b^{\dagger}$ through the channel transformation and tracing over the vacuum modes $a_v^{\dagger}$,$b_v^{\dagger}$, we get the matrix form of $\rho_{ab}(\eta)$ in the Fock basis of the modes a, b. The two classes of states $|\Psi(\sigma)\rangle_{ab}$ and $\rho_{ab}(\eta)$ approach the ideal Dicke state when the parameters σ, η tend to zero.

In the Mach-Zehnder interferometer shown in Fig. 3.4.1 (a), the modes $a_{\pm}$ of the two arms are connected with the input modes a, b by the relation $a_{\pm} = (\pm a + b)/\sqrt{2}$. The phase eigenstates $|\theta_l\rangle_{\pm}$ of the modes $a_{\pm}$ are superpositions of the corresponding Fock states $|n\rangle_{\pm}$ with

$$|\theta_l\rangle_{\pm} = (s+1)^{-1/2} \sum_{n=0}^{s} e^{in\theta_l}|n\rangle_{\pm}$$

where $\theta_l = 2\pi l/(s+1)$ $(l = 0, 1, ..., s)$ and $s+1$ denotes the Hilbert space dimension which eventually takes the infinity limit [52].

For modes $a_\pm$ in a composite state denoted by its density matrix $\rho_\pm$, the probability distribution $P(\theta_r)$ of the relative phase θ_r between the two interferometer arms can be expresses as

$$P(\theta_r) = \sum_{l=0}^{s} {}_\pm\langle \theta_l \theta_{l-\delta l} | \rho_\pm | \theta_l \theta_{l-\delta l} \rangle_\pm, \tag{3.4.1}$$

where $\delta l = \theta_r(s+1)/(2\pi)$.

The phase distribution $P(\theta_r)$ becomes independent of the Hilbert space dimension $s+1$ when s goes to infinity, and the half width $\Delta\theta$ of $P(\theta_r)$ gives an indicator of the intrinsic interferometer sensitivity to measure the relative phase shift for the given input state [24, 50]. We use $\Delta\theta$ to quantify the phase sensitivity for our input states.

In Fig. 3.4.2, we show the calculated phase sensitivity $\Delta\theta$ for the two classes of input states $|\Psi(\sigma)\rangle_{ab}$ and $\rho_{ab}(\eta)$, by varying the parameters σ, η and the particle number N. With fixed parameters σ, η, when we vary the particle number N (typically from 20 to 200 in our calculation), the phase sensitivity $\Delta\theta$ follows a linear dependence with the parameter $\sqrt{\xi_D/N}$ by $\Delta\theta = \alpha\sqrt{\xi_D/N}$ (note that the Dicke squeezing parameter ξ_D changes widely as we vary N and σ, η). The slope α depends very weakly on the parameters σ, η as shown in Fig. 2(c) and 2(d) and roughly we have $\alpha \approx 2$. This shows that for different types of input states the phase sensitivity $\Delta\theta$ is always determined by the parameter $\sqrt{\xi_D/N}$ up to an almost constant prefactor α.

3.5 The Bayesian Inference Method

A good phase sensitivity $\Delta\theta$ is an indicator of possibility of high-precision measurement of the relative phase shift θ, however, the sensitivity by itself does not give the information of θ. In particular, for the DS states we typically have $\left\langle \vec{J} \right\rangle = 0$ and therefore cannot read out the information of θ by measuring rotation of the mean value of $\vec{J}$.

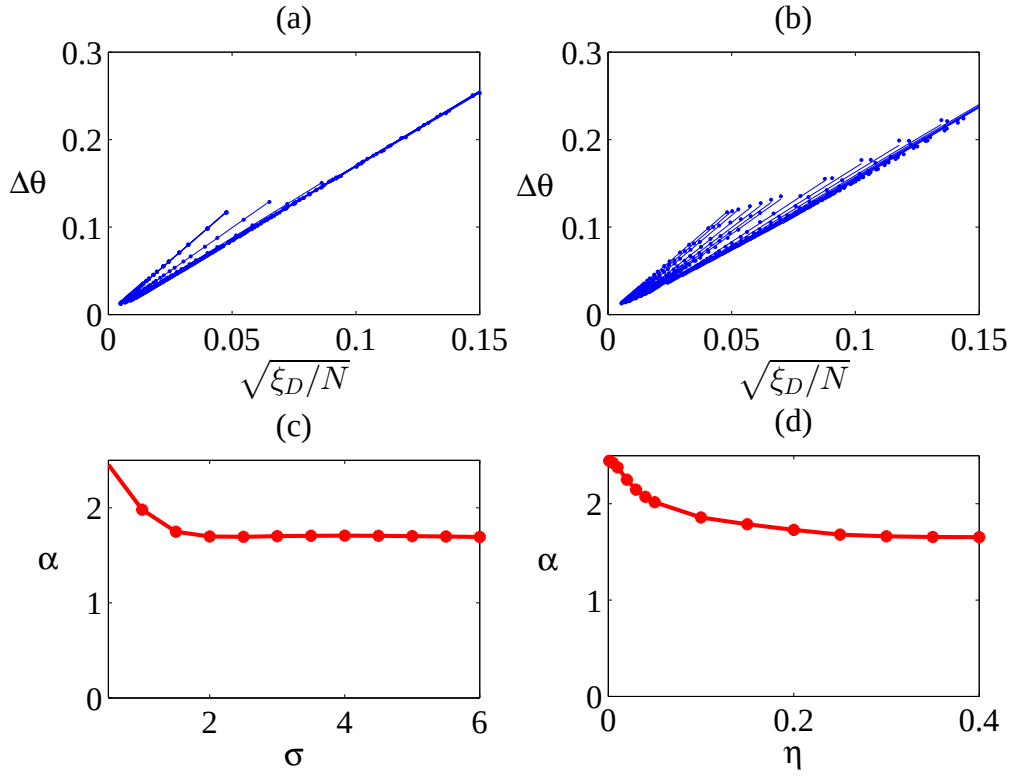

Figure 3.4.2: The phase sensitivity $\Delta\theta$ versus the normalized Dicke squeezing $\sqrt{\xi_D/N}$ for two classes of input states: (a) States $|\Psi(\sigma)\rangle_{ab}$ with Gaussian superposition coefficients. (b) Dissipative states $\rho_{ab}(\eta)$ after a loss channel. The resulting points are on a straight line when we vary the particle number N from 20 to 200 (ξ_D changes correspondingly) and the slope of the line changes slightly as we vary the parameter σ (from 0 to 6) or η (from 0 to 0.4). (c) and (d) show the variation of the slope α as a function of the parameter σ or η.

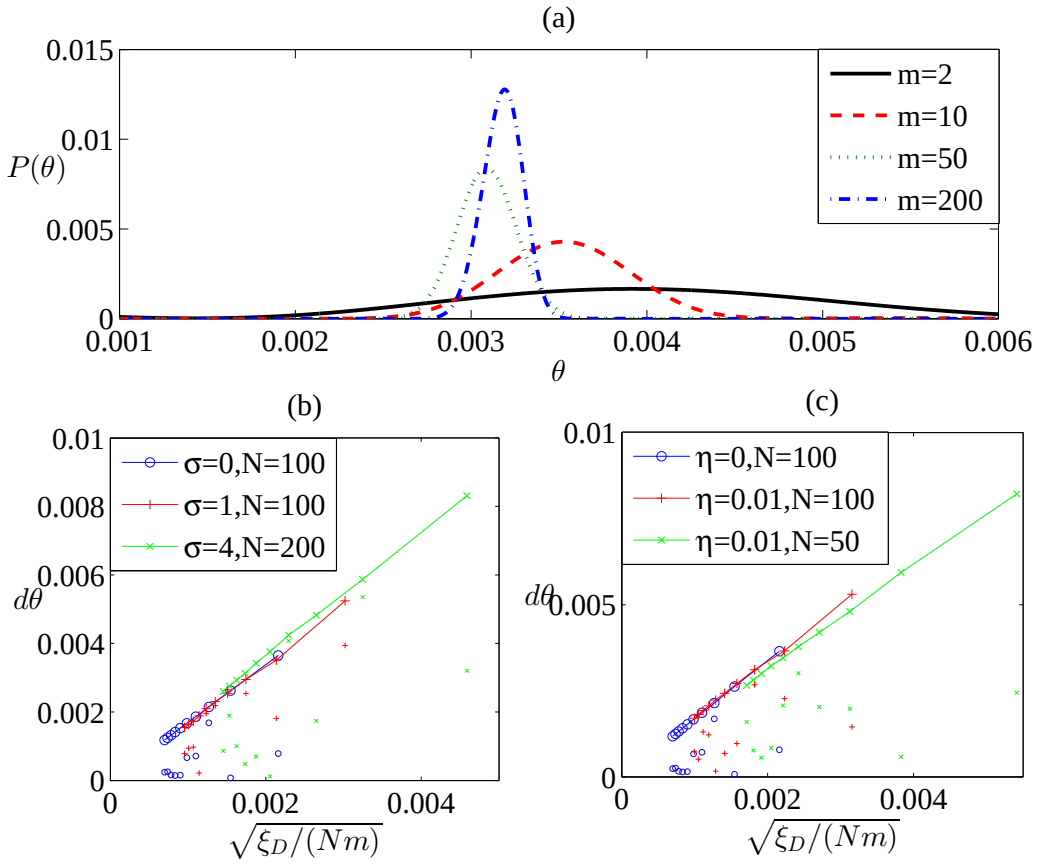

Figure 3.4.3: (a) The posterior phase distributions $P_m(\theta|\{j_z\}_m)$ obtained from the Bayesian inference after the mth measurement with $m = 2, 10, 50$ and 200 from our numerically simulated experiments. In the simulation, the actual phase shift $\theta_r = 0.003$ and the input state is $|\Psi(\sigma)\rangle_{ab}$ with $N = 1000$, $\xi_D = 0.0019$ and $\sigma = 1$. (b) and (c): The measurement precision $d\theta$ (the dots along a line fit by $d\theta \approx 1.7\sqrt{\xi_D/(Nm)}$) and the estimation error θ_{pr} (the scattered points below the line) as functions of the scaled parameter $\sqrt{\xi_D/(Nm)}$ for the Gaussian input states $|\Psi(\sigma)\rangle_{ab}$ (b) and the dissipative input states $\rho_{ab}(\eta)$ (c) with m varying from 20 to 200. The other parameters (σ, N for $|\Psi(\sigma)\rangle_{ab}$ and η, N for $\rho_{ab}(\eta)$) are specified by the inserts of the figure.

A powerful way to read out the information of θ is through the Bayesian inference [24, 50]. Here, we show that with the Bayesian inference, we can faithfully extract the information of θ with a measurement precision $d\theta = \beta\sqrt{\xi_D/N}$ for the DS states, where the prefactor $\beta \approx 1.7$.

We note that each instance of measurement by the MZ interferometer setup shown in Fig. 3.4.1 records one particular eigenvalue j_z of the J_z operator, which occurs with a probability distribution $P(j_z|\theta)$ (called the likelihood) that depends on the relative phase shift θ. With a given input state ρ_{ab} for the modes a, b, the likelihood $P(j_z|\theta)$ is given by .

$$P(j_z|\theta) = \langle j, j_z|e^{i\theta J_y}\rho_{ab}e^{-i\theta J_y}|j, j_z\rangle, \tag{3.5.1}$$

where $|j, j_z\rangle$ denotes the momentum eigenstate with $j = N/2$.

The Bayesian inference is a way to use the Bayes' rule to infer the posterior distribution $P_m(\theta|\{j_z\}_m)$ of the phase shift θ after m instances of measurements of the J_z operator with the measurement outcomes $\{j_z\}_m = j_{z1}, j_{z2}, \cdots, j_{zm}$, respectively.

After the mth measurement with outcome j_{zm}, the phase distribution $P_m(\theta|\{j_z\}_m)$ is updated by the Bayes' rule

$$P_m(\theta|\{j_z\}_m) = \frac{P(j_{zm}|\theta)P_{m-1}(\theta|\{j_z\}_{m-1})}{P(j_{zm}|\{j_z\}_{m-1})}, \tag{3.5.2}$$

where $P(j_{zm}|\{j_z\}_{m-1}) = \int d\theta P(j_{zm}|\theta)P_{m-1}(\theta|\{j_z\}_{m-1})$ is the probability to get the outcome j_{zm} conditional on the sequence $\{j_z\}_{m-1}$ for the previous $m-1$ measurement outcomes.

Before the first measurement, the prior distribution $P_0(\theta)$ is assumed to be a uniform distribution between 0 and 2π. When the instances of measurements $m \gg 1$, the posterior distribution $P_m(\theta|\{j_z\}_m)$ is typically sharply peaked around the actual phase shift, and we use the half width $d\theta$ of $P_m(\theta|\{j_z\}_m)$ to quantify the measurement precision.

To show that the measurement precision $d\theta$ is indeed determined by $\sqrt{\xi_D/N}$ for the DS states,

we numerically simulate the MZ experiment with a randomly chosen actual phase shift θ_r in the interferometer.

We take input states of the forms of $|\Psi(\sigma)\rangle_{ab}$ or $\rho_{ab}(\eta)$ as we specified before, with the corresponding likelihood $P(j_z|\theta)$ given by Eq. (3.5.1). With this likelihood, we get a sequence of measurement outcomes $j_{z1}, j_{z2}, \cdots, j_{zm}$, which are sampled in our numerically simulated experiments using the corresponding probability distributions $P(j_{zk}|\{j_z\}_{k-1})$ with $k = 1, 2, \cdots, m$, respectively.

For this sequence of outcomes, we obtain the corresponding sequence of posterior phase distributions $P_m(\theta|\{j_z\}_m)$, with an example shown in Fig. 3.4.3 (a). One can see that the distribution $P_m(\theta|\{j_z\}_m)$ indeed gets increasingly sharper with m and its peak approaches the actual phase shift θ_r. We use the the central peak position θ_p of the distribution $P_m(\theta|\{j_z\}_m)$ as an estimator of the measured phase shift, and the difference $\theta_{pr} = |\theta_p - \theta_r|$ therefore quantifies the measurement error. This error θ_{pr} is typically bounded by $d\theta$, indicating there is no systematic bias by this inference method.

In Fig. 3.4.3 (b) and 3.4.3(c), we show the measurement precision $d\theta$ and the estimation error θ_{pr} as functions of the scaled parameter $\sqrt{\xi_D/(Nm)}$, as we vary the types of input states (the parameters σ, η in states $|\Psi(\sigma)\rangle_{ab}$ and $\rho_{ab}(\eta)$), the particle number N, and the number of measurement instances m. All the points for the measurement precision $d\theta$ can be well fit with a linear function $d\theta \approx \beta\sqrt{\xi_D/(Nm)}$ with $\beta \approx 1.7$.

The estimation error θ_{pr} from the simulated experiments (the scattered points) is typically below the corresponding $d\theta$. This supports our central claim: the defined Dicke squeezing parameter ξ_D characterizes the improvement of measurement precision for the DS states compared with the standard quantum limit.

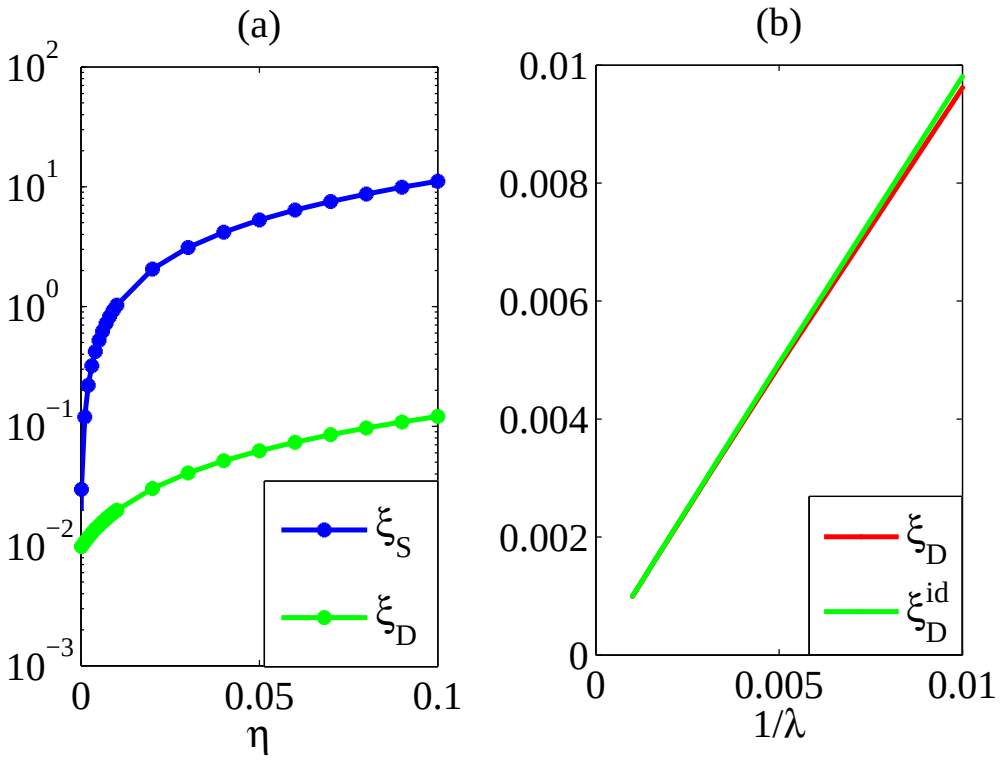

Figure 3.5.1: (a) Comparison of the spin squeezing ξ_S and the Dicke squeezing ξ_D under influence of the particle loss with a loss rate η. We take the particle number $N = 100$ and the amounts of squeezing for ξ_S and ξ_D comparable initially at $\eta = 0$. (b) Comparison of the Dicke squeezing ξ_D for a Poisson distributed mixed state and for a Dicke state with the same mean particle number λ.

3.6 The Noise Robustness

Compared with other entangled states used in quantum metrology, a remarkable advantage of the DS states characterized by the squeezing parameter ξ_D is its noise robustness. For instance, if the noise in experiments is dominated by the dephasing error that does not change the mode population, the numerator does not change in the definition equation (3.3.1) for the Dicke squeezing ξ_D and only the denominator drops slowly.

With a dephasing rate p (p is the probability for each qubit to become completely decoherent), the squeezing parameter reduces to $\xi_D = 1/\left[N(1-p)+2-p^2\right]$ if we start with a Dicke state for N particles [30]. We still have substantial squeezing when $N \gg 1$ even if the dephasing error rate $p \gtrsim 50\%$.

More generic noise such as particle loss has bigger influence on the Dicke squeezing, however, the DS states are still more robust compared with other forms of entangled states such as the spin squeezed states. In Fig. 3.5.1 (a), we show the influence of the particle loss to the Dicke squeezing ξ_D and the spin squeezing ξ_S, starting with comparable values of ξ_S and ξ_D at the loss rate $\eta = 0$ under the same particle number N. The spin squeezed state was determined by minimizing $(\Delta J_z)^2$ with $J_x = 0.1J$ [21]. One can see that that the spin squeezing ξ_S is quickly blown up by very small particle loss, but substantial Dicke squeezing ξ_D remains even under a significant loss rate. In the asymptotic limit with $N \gg 1$, $\xi_D \approx \eta/(1-\eta)$ under a loss rate η. Therefore, compared with the standard quantum limit, the measurement precision improves by a constant factor of $\sqrt{\xi_D} \approx \sqrt{\eta/(1-\eta)}$ for the DS state under loss. This has saturated the bound derived in Ref. [53], which proves that under noise the measurement procession can be improved at most by a constant factor for any quantum entangled states (the factor is exactly $\sqrt{\eta/(1-\eta)}$ under a loss rate η as proven in [53]).

The saturation of the improvement bound shows that the DS states characterized by the parameter

ξ_D belong to the optimal class of states for improving the measurement precision under noise (note that the conventional spin squeezed states measured by the squeezing parameter ξ_S are not optimal for improving measurement precision under noise as ξ_S is quickly blown up to be larger than 1 (see Fig. 3.5.1 (a)), yielding no improvement compared with the standard quantum limit). In Fig. 3.5.1 (b), we consider an initial mixed state prepared in experiment with variable particle number. The particle number is Poisson distributed with the probability for n particle as $P(n) = \frac{\lambda^n e^{-\lambda}}{n!}$, so the mean particle number of the system is $\langle N \rangle = \lambda$. ξ_D for this initial state is compared with that for the Dicke states of the same mean particle number λ. From the plot we can see the difference is small and ξ_D is insensitive to the input state number fluctuation.

3.7 Chapter Summary

In summary, we have proposed a new class of many-particle entangled states characterized by the introduced Dicke squeezing parameter ξ_D to improve the measurement precision in quantum metrology. We show that the phase information can be read out through the Bayesian inference and the measurement precision is improved by a factor of $\sqrt{\xi_D}$ compared with the standard quantum limit.

A distinctive advantage of the DS states is its noise robustness and we show that the Dicke squeezing ξ_D is much more robust compared with other forms of entangled states used in quantum metrology. Substantial Dicke squeezing can be generated in experiments, for instance, through the atomic collision interaction in spinor condensates [34, 54]. With the characterization and measurement method proposed in this paper, the Dicke squeezing may lead to a fruitful approach for precision quantum metrology using entangled quantum states.

This chaper contains content that was published elsewhere [55] and is available at

http://iopscience.iop.org/1367-2630/16/10/103037.

CHAPTER IV

Quantum Metrology Using Spin Squeezed State

4.1 Background Information

The precise measurement of phase is an important issue for both theoretical and experimental studies [35–38]. As well as a fundamental question itself, searching of quantum states with high phase precision is also required for an atomic clock. Systems with strong quantum entanglement are believed to have higher phase precision and therefore offer a good candidate for atomic clocks. Among all the entangled states, spin squeezed states have promising performance [8]. Effective methods for the preparation of spin squeezed states and their application in quantum metrology are proposed in various experiment platforms [9, 10, 43–46, 56].

For a system of N spin half particles, the collective spin operator $\overrightarrow{J}$ can be expressed by the Pauli matrix $\overrightarrow{\sigma_i}$ of each single qubit as $\overrightarrow{J} = \sum_i \overrightarrow{\sigma_i}/2$. The spin squeezed states are defined as states with minimized noise ΔJ_z for a given value of $\langle J_x \rangle$. Those states have small fluctuation for their internal phases, so they can be used in quantum metrology. It is shown that the the phase resolution of N spin-$1/2$ atoms contains the factor $\xi_s = \frac{N\langle(\Delta J_z)^2\rangle}{\langle J_x\rangle^2}$ [21], and ξ_s can also be used to characterize the entanglement property as $\xi_s < 1$ indicates that there is manybody entanglement in the system [18].

However ξ_s is very sensitive to experimental noise. For states with small $\langle J_x \rangle$, fluctuation in the particle number will cause uncertainty in the spin $\delta\langle J_x \rangle$ comparable to $\langle J_x \rangle$ and this can result in non-negligible change of ξ_s. Also for the maximally entangled Dicke state $|J = \frac{N}{2}, J_z = 0\rangle$, ξ_s fails to characterize the entanglement as both $\langle (\Delta J_z)^2 \rangle$ and $\langle J_x \rangle$ go to zero.

In this chapter we introduced a new parameter ξ_n considering the properties of spin squeezed states and proved that ξ_n can work as a proper characterization of the phase precision for spin squeezed states and is more robust to experimental noise.

4.2 Definition of the Squeezing Parameter ξ_n

To analyze the phase sensitivity of spin squeezed states, we illustrate the state rotation of an angle θ in the y direction in Fig.4.2.1. The measurement sensitivity of the rotation angle θ is decided by the spin distribution of the state in the Bloch sphere in the x direction and its fluctuation in the z direction, and the sensitivity is maximized if the spin distribution has a wide spread in the x direction and a small fluctuation in the z direction. So using a parameter containing $\langle J_x^2 \rangle$ and $\langle (\Delta J_z)^2 \rangle$ to describe the phase sensitivity is a reasonable choice.

The phase sensitivity is also related to the entanglement property of the state. While $\xi_s < 1$ indicates entanglement in the system, we would like to construct a squeezing parameter which can quantify the the amount of entanglement. We consider an entangled N qubit system described by the density matrix $\rho = \sum_\mu p_\mu \rho_\mu$, with $p_\mu \geq 0$ and $\sum_\mu p_\mu = 1$. If there is no genuine $(m_0 + 1)$-qubit entanglement ρ_μ can be decomposed in the form of $\rho_\mu = \rho_{1\mu} \otimes \rho_{2\mu} \otimes \cdots \otimes \rho_{k\mu}$, where $\rho_{i\mu} (i = 1, 2, \cdots, k)$ represents a component state of $m_{i\mu}$qubits with $\sum_{i=1}^{k} m_{i\mu} = N$ and $1 \leq m_{i\mu} \leq m_0$. From Eq. (6) of Duan's paper in 2011 [30], the following inequation holds

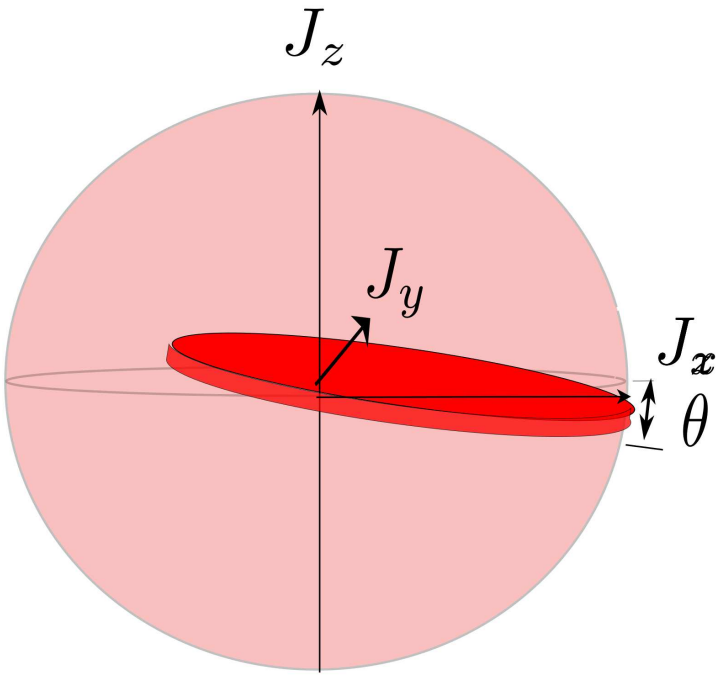

Figure 4.2.1: In the Bloch sphere for the collective spin operator $\vec{J}$, the phase precision is represented by the rotation of a thin disk (its size in x, y, z directions corresponds to the variance of $\vec{J}$) of an angle θ in the y direction.

$$\langle J_x^2\rangle \leq \sum_{\mu,i} p_\mu [\langle (\Delta J_{xi})^2\rangle_\mu + 4\langle (\Delta J_z)^2\rangle_\mu \langle (\Delta J_{yi})^2\rangle_\mu].$$

As $\langle (\Delta J_{\alpha i})^2\rangle_\mu \leq \langle J_{\alpha i}^2\rangle_\mu \leq m_{i\mu}^2/4$ for $\alpha = x,y,z$, $(\sum_i \langle J_{xi}\rangle)_\mu^2 \leq k\sum_i \langle J_{xi}\rangle_\mu^2$ and $\langle (\Delta J_z)^2\rangle \geq \sum_\mu p_\mu \langle (\Delta J_z)^2\rangle_\mu$, we have

$$\begin{aligned}
\langle J_x^2\rangle + \frac{\langle J_x\rangle^2}{N} &\leq \sum_\mu p_\mu [\sum_i \langle (\Delta J_{xi})^2\rangle_\mu + \frac{\sum_i \langle J_{xi}\rangle_\mu^2}{N} + 4\langle (\Delta J_z)^2\rangle_\mu \langle (\Delta J_{yi})^2\rangle_\mu] \\
&\leq \sum_\mu p_\mu [\sum_i \langle J_{xi}^2\rangle_\mu + (\frac{k}{N} - 1)\sum_i \langle J_{xi}\rangle_\mu^2 + 4\langle (\Delta J_z)^2\rangle_\mu \langle (\Delta J_{yi})^2\rangle_\mu] \\
&\leq \sum_\mu p_\mu [\sum_i \frac{m_{i\mu}^2}{4}(1 + 4\langle (\Delta J_z)^2\rangle_\mu)] \\
&\leq [1 + 4\langle (\Delta J_z)^2\rangle] \max_{\{m_{i\mu}\}} (\sum_i \frac{m_{i\mu}^2}{4}). \qquad (4.2.1)
\end{aligned}$$

This maximum value is obtained when we choose $k = [\frac{N}{m_0}]$ where $[\frac{N}{m_0}]$ is the largest integer no less than $\frac{N}{m_0}$, $m_{1\mu} = N - m_0(k-1)$, and all the other $m_{i\mu} = m_0$, and correspondingly the above equation is reduced to

$$\langle J_x^2\rangle + \frac{\langle J_x\rangle^2}{N} \leq [1 + 4\langle (\Delta J_z)^2\rangle] m_0 N/4. \qquad (4.2.2)$$

This inequation indicates that if we define a squeezing parameter

$$\xi_n = \frac{N(\langle (\Delta J_z)^2\rangle + \frac{1}{4})}{\langle J_x^2\rangle + \frac{\langle J_x\rangle^2}{N}},$$

for a state without genuine (m_0+1)-particle entanglement the inverse of ξ_n is bounded by m_0 with $\frac{1}{\xi_n} \leq m_0$.

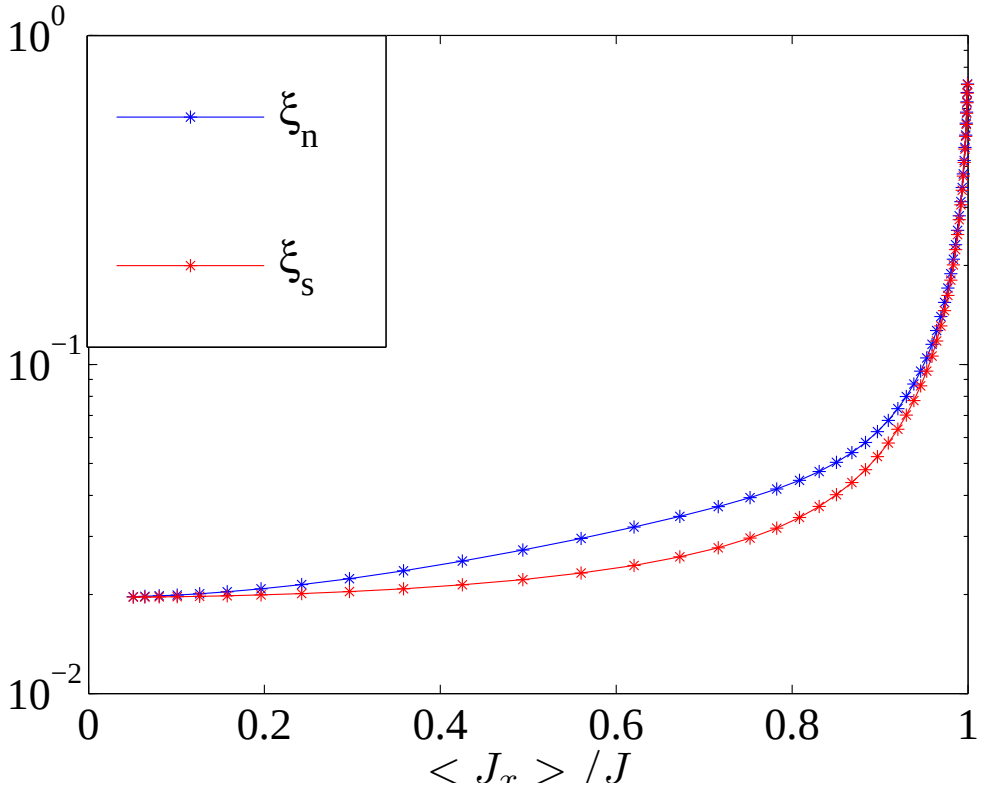

Figure 4.2.2: Comparison of ξ_s and ξ_n for spin squeezed states with $\langle J_x \rangle / J$ from zero to unity. The difference between ξ_s and ξ_n is small and turns to zero at the two ends of zero $\langle J_x \rangle$ and maximum $\langle J_x \rangle$. The value of ξ_s at $J_x = 0$ is not shown as at this point ξ_s is unstable. The particle number of the system is $N = 100$.

This squeezing parameter ξ_n contains $\langle (\Delta J_z)^2 \rangle$ and $\langle J_x^2 \rangle$, as we predicted above from the Bloch sphere analysis. An extra $\frac{\langle J_x \rangle^2}{N}$ term in the denominator insures that ξ_n goes to unity for the spin coherent state with spin of all atoms pointing to the x direction. As shown in Fig. 4.2.2, the difference between ξ_s and ξ_n is small for spin squeezed states with $\langle J_x \rangle$ from 0 to the maximum value of $J = N/2$.

4.3 Method for Precision Measurement

The Mach-Zehnder interferometer offers a method to reach the Heisenberg limit of sensitivity for the measurement of the phase difference θ between two light beams in an optical system [24], when the input state has strong quantum entanglement, such as the Dicke state $|J = \frac{N}{2}, J_z = 0\rangle$. Taesoo Kim [50] generalized this idea to all quantum coherent system such as trapped ions [39] or atomic interferometry with Bose condensates [57]. The correspondence between this phase shift of an optical light beam and the rotation of a spin system is also stated.

Spin squeezed states can be used in this high sensitivity phase measurement method with their small internal phase fluctuation. However a powerful detection method of the rotation angle is still needed. A simple measurement of $\langle J_z \rangle$ or $\langle J_z^2 \rangle$ could not give out high precision information of the rotation angle θ as the fluctuation of J_z and J_z^2 themselves are comparable to their mean values.

Holland and Burnett proposed an effective method to read out the phase information of the Dicke state by using Bayesian inference [24]. We know that after a rotation of angle θ in the y direction, the values of J_z detected obey the probability distribution $P(J_z|\theta)$ that depends on θ. If the state before rotation is ψ_{ss}, $P(J_z|\theta)$ then has the distribution of

$$P(J_z|\theta) = |\langle J, J_z | e^{i\theta J_y} | \psi_{ss} \rangle|^2 \tag{4.3.1}$$

where $|J, J_z\rangle$ is the eigenstate of J_z with $J = N/2$. The estimated θ after m instances of measurements of J_z can be derived by using the Bayer's rule as

$$P_m(\theta|\{J_z\}_m) = \frac{P(J_{zm}|\theta) P_{m-1}(\theta|\{J_z\}_{m-1})}{P(J_{zm}|\{J_z\}_{m-1})} \tag{4.3.2}$$

with the outcomes of the m measurements as

$$\{J_z\}_m = J_{z1}, J_{z2}, \cdots, J_{zm}$$

and the denominator

$$P(J_{zm}|\{J_z\}_{m-1}) = \int d\theta P(J_{zm}|\theta) P_{m-1}(\theta|\{J_z\}_{m-1})$$

as the probability for the outcome J_{zm} when the previous $m-1$ measurement outcomes are known. $P(J_{zm}|\{J_z\}_{m-1})$ works as a normalization factor here.

For $m = 1$, there is no prior knowledge about θ so we take $P_0(\theta|\{J_z\}_0)$ as an uniform distribution between 0 and 2π. After several measurement the distribution $P_m(\theta|\{J_z\}_m)$ contracts to a sharp peak around a central value θ_p, and the half width $d\theta$ of this distribution is used as the phase measurement precision.

To test the behavior of $d\theta$, we simulate the measurement process numerically with the spin squeezed state of various $\langle J_x \rangle$ as the input states, and make a randomly chosen rotation angle around the y axis. The measurement result of the spin J_z then has the distribution probability $P(J_z|\theta)$ as shown in Eq. (4.3.2). After we get m measurement outcomes $J_{z1}, J_{z2}, \ldots, J_{zm}$, the probability distribution of the rotation angle θ is calculated recursively using Eq. (4.3.2).

The shape of $P_m(\theta|\{J_z\}_m)$ goes to a sharp peak around the central position θ_p and the half width $d\theta$ is small when measurement number m is large enough. θ_p is then taken as an estimator for the measured rotation angle and it should approach the actual rotation angle θ_r after infinite number of measurement. An example of the corresponding distributions $P_m(\theta|\{J_z\}_m)$ for a sequence of measurement outcomes $J_{z1}, J_{z2}, \ldots, J_{zm}$ are calculated and are shown in Fig. 4.3.1 (a) for certain measurement sequences of $m = 1, 2, 5, 10, 50$ and 100, with the input state as a spin squeezed state

of 10^3 particles and $\langle J_x \rangle = 0.1J$.

Fig. 4.3.1 (b) shows the half width $d\theta$ and the measurement error $\theta_{pr} = |\theta_p - \theta_r|$ as functions of the scaled parameter $\sqrt{\xi_n/(Nm)}$ with the green straight line representing $d\theta$ and the random purple dots for θ_{pr}. As we predicted the measurement precision $d\theta$ has a linear relation with $\sqrt{\xi_n/(Nm)}$ and thus is determined by $\sqrt{\xi_n/N}$ for spin squeezed states. The measurement error θ_{pr} is typically bounded by $d\theta$ as shown in the figure.

To confirm the relation of $d\theta$ and $\sqrt{\xi_n/N}$, in Fig.4.3.2 we show the behavior of $d\theta$ with decreasing $\sqrt{\xi_n/(Nm)}$ for several spin squeezed states of different values of $\langle J_x \rangle$ as the input states and the rounds of measurement m varied from 20 to 100. Similar to the result in [55], for all input states $d\theta$ and $\sqrt{\xi_n/(Nm)}$ has a linear relation as $d\theta \approx \beta\sqrt{\xi_n/(Nm)}$ with the fitted coefficient $\beta \approx 1.2$. This linear fitting confirms that the defined squeezing parameter ξ_n is a characterization of the phase measurement precision for the spin squeezed states.

4.4 Noise Discussion

The noise in experiments will have influence on ξ_n, and thereby on the phase precision. In the following we discuss the robustness of ξ_n under various noises.

The first kind of noise under consideration is the dephasing noise, which is a major source of error in many experiments. ξ_n is robust to dephasing as phase decoherence does not change the mode population, so there is no increase in $\langle (\Delta J_z)^2 \rangle$. For spin squeezed states with $\langle J_x \rangle / J > 0.8$, the squeezing is small as ξ_n gets large and comparable to 1, thus states with large $\langle J_x \rangle$ is not useful in metrology. So here we consider the change of ξ_n with spin squeezed states of small $\langle J_x \rangle / J$. With $N = 10^3$, $\langle (\Delta J_z)^2 \rangle < 1$ for these states.

To estimate the value of ξ_n, we assume a dephasing error rate p for each individual qubit. As

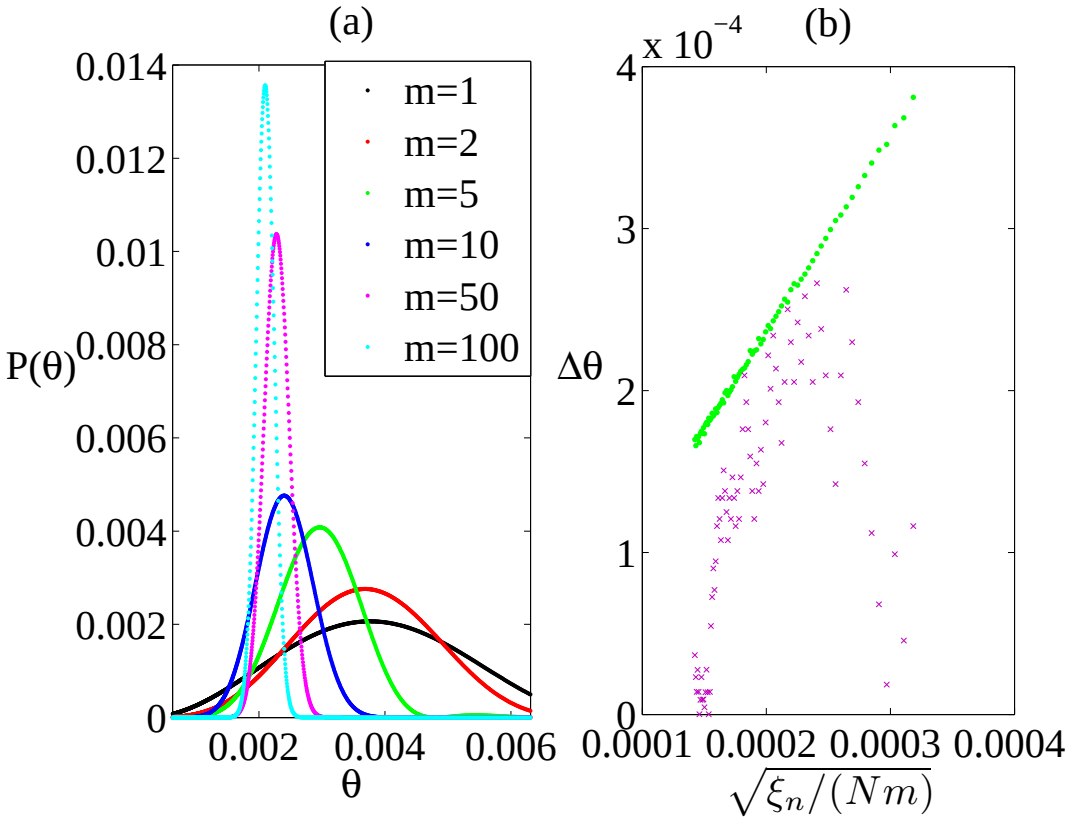

Figure 4.3.1: (a): The calculated phase distribution $P_m(\theta|\{J_z\}_m)$ from Bayesian interference after the mth measurement with $m = 1,2,5,10,50$ and 100 from simulated experiment data. The simulation is implemented with an initial spin squeezed state of $\langle J_x\rangle = 0.1J$, $\xi_n = 2.03\times 10^{-3}$ and $N = 10^3$, and the actual phase shift is chosen as $\theta_r = 0.002$. (b): The simulated process with the number of measurement instances m from 20 to 100 with a spin squeezed state of $\langle J_x\rangle = 0.1J$, $\xi_n = 2.03\times 10^{-3}$ and $N = 10^3$. Green line is the measurement precision $d\theta$ and the scattered purple points are the estimation error θ_{pr}.

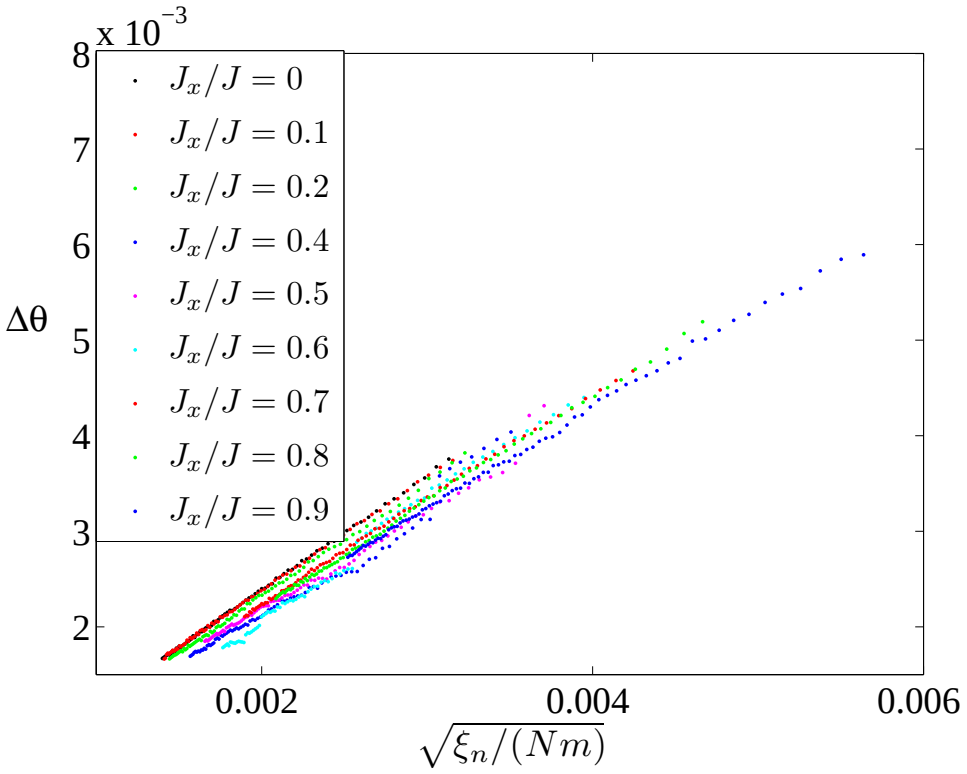

Figure 4.3.2: The measurement precision $d\theta$ as a function of the scaled parameter $\sqrt{\xi_n/(Nm)}$ for spin squeezed state with various $\langle J_x \rangle / J$. The round of measurement m varies from 20 to 100 and the system's particle number is $N = 100$.

before we expand the spin squeezed state ψ_{ss} in the basis of J_z's eigenstates. If the dephasing rate $p = 1$, which means complete dephasing, for each term of J_z's eigenstate we have $\langle J_x^2 \rangle = \sum_{i=1}^{N} \langle (\sigma_{ix}/2)^2 = N/4$. This leads to $\xi_n \sim 1$ indicating no squeezing in the state. When $p < 1$, the state follows a probability of a binomial distribution $P_i = \begin{pmatrix} N \\ i \end{pmatrix} p^i (1-p)^{N-i}$ for i qubits to be decohered. This results in $\langle J_x^2 \rangle_i = \frac{i}{4}$ for the subsystem of i qubits. For the remaining $N-i$ coherence qubits as $\langle (\Delta J_z)^2 \rangle_{N-i} < 1$ and $\langle J_x^2 \rangle_{N-i} > \langle J_y^2 \rangle_{N-i}$, we expect a minimum $\langle J_x^2 \rangle_{N-i}$ of $\frac{J \cdot (J+1)}{2} = \frac{(N-i)\cdot(N-i+2)}{8}$. And $\langle J_x \rangle$ should be in the order of N. Considering all these changing ξ_n is estimated with a maximum value of

$$\begin{aligned} \xi_n &\sim \frac{cN}{\sum_{i=0}^{N} P_i (\frac{i}{4} + \frac{(N-i)\cdot(N-i+2)}{8}) + \frac{\langle J_x \rangle^2}{N}} \\ &\sim \frac{8c}{N(1-p)^2} \end{aligned}$$

Here c is a constant of $O(1)$ and only terms of order N are left in the denominator. From this estimation even with the dephasing rate $pN \gg 1$, the state is still squeezed and has a relatively high phase measurement precision.

Other noises such as the particle loss noise and the bit-flip error has stronger influence on ξ_n as there is significant increase of $\langle (\Delta J_z)^2 \rangle$. To check the stability of ξ_s in the presence of particle loss noise, we calculated ξ_s for mixed states $\rho(\eta)$ which comes from noise distortion of the squeezed state with a fixed $\langle J_x \rangle$ after a particle loss channel of loss rate η.

This loss channel can be modeled by the transformation $a = \sqrt{1-\eta} a_s + \sqrt{\eta} a_v$ and $b = \sqrt{1-\eta} b_s + \sqrt{\eta} b_v$, where a_s, b_s denote the annihilation operators of the two levels in the spin half atoms and a_v, b_v represent the corresponding vacuum modes. The spin squeezed state can be expressed by $a_s^\dagger$ and $b_s^\dagger$ as

$$\psi_{ss} = \sum_{n=0}^{N} c_n a_s^{\dagger n} b_s^{\dagger (N-n)} |0,0\rangle,$$

here c_n is the coefficient determined by the value of $\langle J_x \rangle$. The density matrix $\rho(\eta)$ is derived by substituting $a_s^\dagger$ and $b_s^\dagger$ with $a^\dagger$ and $b^\dagger$ through the transformation and tracing out the vacuum modes $a_v^\dagger$ and $b_v^\dagger$. $\rho(\eta)$ is reduced to the spin squeezed state of fixed $\langle J_x \rangle$ when η goes to zero and the particle loss effect is more significant when η gets larger. Here we start from a spin squeezed state with $\langle J_x \rangle = 0.1J$ and add the particle loss channel with the loss rate η.

The blue lines in Fig.4.4.1 show the behavior of ξ_s with the loss rate η from 0 to 0.1, with a particle number of $N = 10^3$ and $N = 10^2$ respectively. We can see that even with a strong squeezing, particle loss of $\eta \sim 0.1$ will cause a ξ_s close to 1, which indicates no entanglement in the system.

We believe that the dramatic increasing of ξ_s is caused by the fragility of this parameter and there is still strong manybody entanglement in the squeezed state. The corresponding ξ_n is shown as the red lines in Fig.4.4.1. As we can see the increase of ξ_n is not so obvious as η gets larger, so ξ_n is much more robust than ξ_s under particle loss noise.

To show the robustness of ξ_n under particle loss noise, the precision measurement process is simulated for an initial spin squeezed state of $\langle J_x \rangle = 0.1J$ with a particle loss channel for various rate η. As the input state is represented by the density matrix $\rho(\eta)$, the corresponding probability distribution $P(J_z|\theta)$ thus has a similar form of

$$P(J_z|\theta) = \langle J, J_z | e^{i\theta J_y} \rho(\eta) e^{-i\theta J_y} | J, J_z \rangle \tag{4.4.1}$$

instead of Eq. (4.3.1) of a state vector. With particle loss the dimension for the Hilbert space increases from $N+1$ to $\frac{N(N+1)}{2}$. So we make an approximation of the input state by limiting

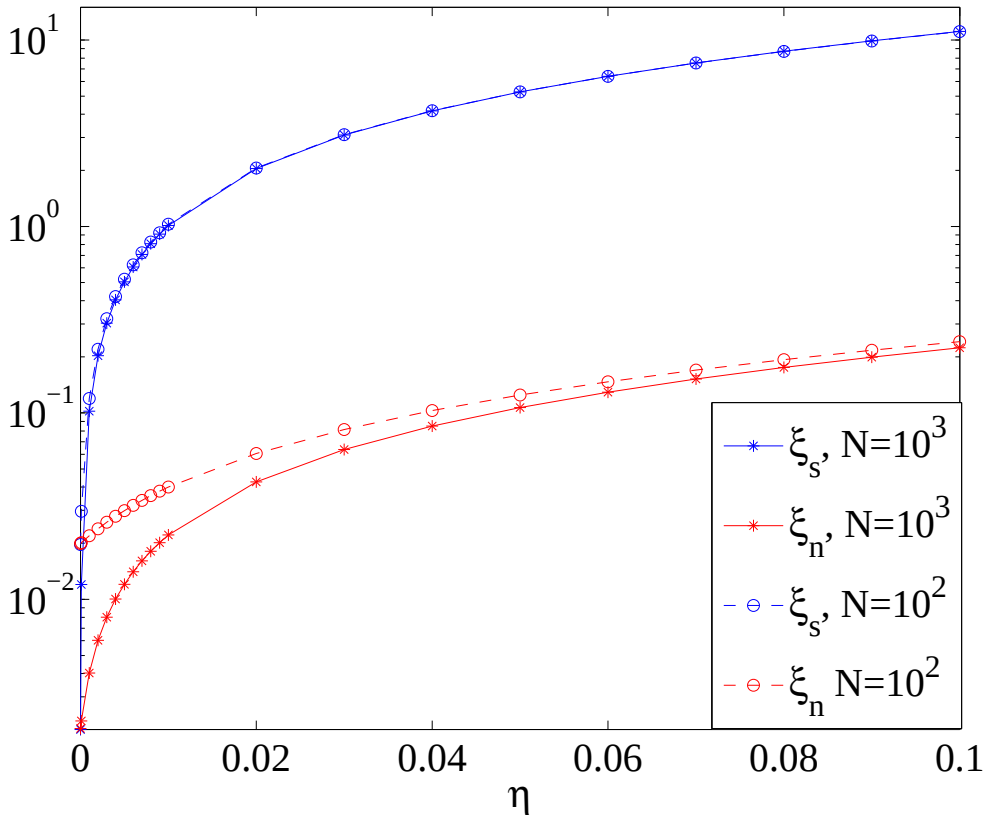

Figure 4.4.1: Comparison of ξ_s and ξ_n under the influence of the particle loss noise with a loss rate η from 0 to 0.1. The particle number of the system is $N = 10^2$ and 10^3 and the spin in the x direction of the initial spin squeezed state is $\langle J_x \rangle / J = 0.1$.

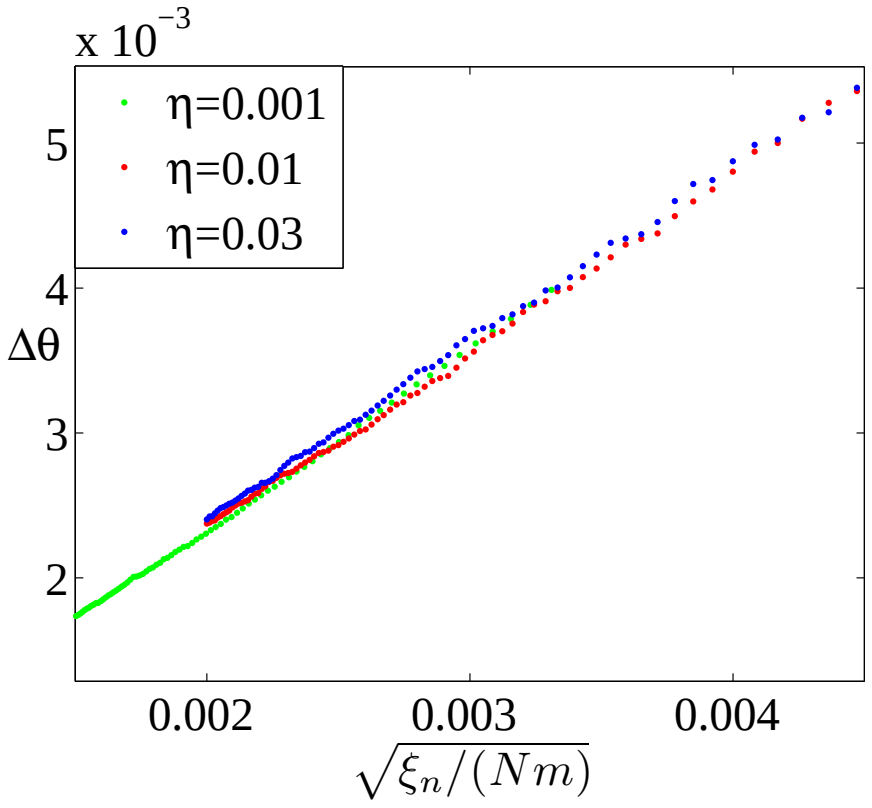

Figure 4.4.2: The measurement precision $d\theta$ as a function of the scaled parameter $\sqrt{\xi_n/(Nm)}$ for spin squeezed state of $\langle J_x\rangle/J = 0.1$ with particle loss of loss rate $\eta = 0.001, 0.01$ and 0.03. The round of measurement m varies from 20 to 100 and the system's particle number is $N = 100$.

the loss number of particle to a maximum of 5 for $\eta = 0.001$ and 0.01 and to a maximum of 8 for $\eta = 0.03$. The expected linear relation of $d\theta$ and $\sqrt{\xi_n/(Nm)}$ is shown in Fig. 4.4.2 with $\eta = 0.001, 0.01$ and 0.03, and the fitted coefficients for all three lines are around 1.2.

When particle loss does not exist, ξ_n is of the order of $\frac{1}{N}$ and the phase sensitivity approaches the Heisenberg limit of $d\theta \sim \frac{1}{N}$. As η increases ξ_n goes to a constant value whose dependence on the system size is very weak as seen in Fig. 4.4.1, and the phase sensitivity $d\theta \sim \frac{1}{\sqrt{N}}$ with a constant factor improvement to the classical limit. This is in correspondence with the discussion in [53].

For the bit-flip noise, We define the bit-flip error rate for each qubit as p_b. If p_b is as weak as $Np_b \ll 1$ the increase in $\langle(\Delta J_z)^2\rangle$ is negligible, so is the change of ξ_n. With an error rate of $Np_b(1-p_b) > 1$, the variance of J_z is estimated by $\langle(\Delta J_z)^2\rangle \sim Np_b(1-p_b)$ for a spin squeezed state with $\langle J_x\rangle/J < 0.8$. This will cause a maximum increase of ξ_n to about $8p_b(1-p_b)$. So with one percent of bit-flip error rate for each qubit it is still possible to demonstrate a squeezing parameter ξ_n of a few percents.

4.5 Chapter Summary

In summary, we have introduced a new spin squeezing parameter ξ_n to better characterize the measurement precision of spin squeezed states, which is more robust compared to ξ_s. We have used the Bayesian method to measure the phase precision for a spin squeezed state and shown that the phase precision is characterized by ξ_n. This method makes important applications of spin squeezed states for quantum metrology. The effect of various noises on ξ_n is also discussed.

CHAPTER V

Boson Sampling with Trapped Ions

5.1 Background Information

What is the ultimate computational power of physical devices? That is a deep question of great importance for both physics and computer science. The famous extended Church-Turing thesis (ECTT) postulates that a (classical) probabilistic Turing machine can efficiently simulate the computational power of any physical devices ("efficiently" here means with a polynomial overhead) [58].

The recent development in quantum computation brings doubt to the ECTT with discovery of superfast quantum algorithms. The most well known example is Shor's algorithm to factorize a large number in polynomial time with a quantum computer [59]. Classically, whether factoring is hard is not settled (a "hard" problem means its solution requires exponential time). No efficient classical algorithm has been found yet to solve factoring, but it wouldn't be very surprising if one finds one as this will not induce dramatic change to the computational complexity theory.

Recently, Ref. [58] introduces another problem, called Boson sampling, which is hard for classical computers but can be solved efficiently with a quantum machine. Boson sampling is defined as a

problem to predict the probabilities of the measurement outcomes in the Fock basis for M Bosonic modes, which start in definite Fock states and undergo a series of mode mixing defined in general by a unitary matrix.

By definition, this problem can be efficiently solved with a quantum machine, but classically its solution requires sampling of a probability distribution given by matrix permanents with an exponentially large number of possible outcomes. Computation of the matrix permanent is known to be #P-hard (much harder than the more well-known class of the NP-hard problems) [60]. Ref. [58] rigorously proved that Boson sampling is classically intractable unless the so-called polynomial hierarchy in the computational complexity theory collapses, which is believed to be extremely unlikely. In this sense, compared with the factoring problem, although Boson sampling has no immediate practical applications, it is a problem much harder for classical computers to solve.

A demonstration of Boson sampling with a quantum machine thus constitutes an effective disproof of the famous ECTT. Because of this far-reaching theoretical implication, experimental demonstration of the Boson sampling has raised strong interest recently. Several publications this year have reported proof-of-principle demonstrations of the Boson sampling with up to three photons [61–64]. The key challenge for the next-step experiments is to scale up the number of Bosons.

The demonstration using photons based on the spontaneous parametric down conversion source has difficulty in terms of scalability [61–64]. The success probability decreases very rapidly with the number of photons due to the probabilistic nature of the single-photon source and the significant photon loss caused by the detector and the coupling inefficiencies. This, in practice, limits the number of Bosons below 10, which is still within the simulation range of classical computers.

In this chapter, we describe a scalable scheme to realize Boson sampling using the transverse phonon modes of trapped ions. Compared with the implementation using photons, this scheme has the following desirable features:

First, the Fock states of the phonons can be prepared in a deterministic fashion and there is no limitation to the number of Bosons that one can realize with this system. We encode the Bosons using the local transverse phonon modes [47], and the state initialization can be done through simple Doppler cooling and one step of the sideband cooling that applies to any number of ions.

Second, we find a technique to do projective detection of the phonon numbers for all the ions through sequential spin quantum jump measurements. This gives an implementation of number-resolving phonon detectors with near perfect efficiency, much higher than the efficiency of typical single-photon detectors. Finally, we prove that universal coherent mixing of different phonon modes can be achieved through a combination of the inherent Coulomb interaction and simple laser-induced phase shifts of the ions.

Through this scheme, it is feasible to realize Boson sampling for tens of phonons with the state-of-the-art trapped ion technology. This scale has gone beyond the simulation capability of any classical computers and corresponds to the most interesting experimental region for test of the ECTT [65, 66].

5.2 Basic Idea

The problem of Boson sampling is defined as follows: we have M input Bosonic modes a_i ($i = 1, 2, ..., M$), which undergo coherent mode mixing described in general by a unitary matrix Λ, with the output modes given by $b_i = \sum_j^M \Lambda_{ij} a_j$. The input modes are prepared in a Fock (number) state $|\mathbf{T}\rangle = |t_1, t_2, ..., t_M\rangle$, where t_i is an integer denoting the occupation number of the mode a_i. We measure the output modes b_i in the Fock basis and the probability to get the outcome $|\mathbf{S}\rangle =$

$|s_1, s_2, ..., s_M\rangle$ is given by [58, 67]

$$P(\mathbf{S}|\mathbf{T}) = \frac{\left|Per\left(\Lambda^{(\mathbf{S},\mathbf{T})}\right)\right|^2}{\prod_{j=1}^{M} s_j! \prod_{i}^{M} t_i!} \tag{5.2.1}$$

where $Per(\cdot)$ denotes the matrix permanent and $\Lambda^{(\mathbf{S},\mathbf{T})}$ is a sub-matrix of Λ formed by taking s_j copies of the j-th column and t_i copies of the i-th row of the matrix Λ. Since the total number of Bosons is conserved $N = \sum_i^M a_i^\dagger a_i = \sum_j^M b_j^\dagger b_j$, the sub-matrix $\Lambda^{(\mathbf{S},\mathbf{T})}$ has dimension $N \times N$.

Due to the hardness to calculate the matrix permanent, it becomes impossible to sample the probability distribution $P(\mathbf{S}|\mathbf{T})$ with any classical computer when the number of Bosons N increases beyond $20 \sim 30$. An experimental demonstration of a quantum machine that can successfully perform this job therefore provides strong evidence against the ECTT.

5.3 Trapped Ion Realization

To realize Boson sampling with trapped ions, we consider a chain of ions in a linear Paul trap with the transverse trapping frequency ω_x significantly large than the axial one ω_z. The Bosons are represented by the local transverse phonon modes a_i associated with each ion i ($i = 1, 2, ..., M$), all with the oscillation frequency ω_x.

The Coulomb interaction between the ions introduces a small perturbation to the oscillation frequency of the local phonon modes, with the interaction Hamiltonian described by [68, 69]

$$H_c = \sum_{1 \le i < j \le M} \hbar t_{i,j} \left(a_i^\dagger a_j + a_i a_j^\dagger\right), \tag{5.3.1}$$

where the hopping rates $t_{i,j} = t_0 / \left|z_{i0} - z_{j0}\right|^3$ and $t_0 = e^2/(8\pi\varepsilon_0 m\omega_x)$. Here, z_{i0} denotes the axial equilibrium position of the ith ion with mass m and charge e. The Hamiltonian (5.3.1) is valid under

the condition $t_{i,j} \ll \omega_x$, which is always satisfied for the parameters considered in this chapter.

To make the scheme more scalable and eliminate the challenging requirement of resolving phonon sidebands for a large ion chain, we use the local transverse phonon modes to represent the target Bosons instead of the conventional normal modes.

To initialize the local phonon modes a_i to the desired Fock states, first we cool them to the ground state by laser cooling. The routine Doppler cooling achieves a temperature $T_D \sim \hbar\Gamma/(2k_B)$ (Γ is the natural bandwidth of the excited state and k_B is the Boltzmann constant), with the corresponding thermal phonon number $\bar{n}_x = k_B T_D/\hbar\omega_z \sim \Gamma/(2\omega_x)$, which is about $1 \sim 2$ under typical values of $\omega_x \approx 2\pi \times (5 \sim 10)$ MHz and $\Gamma \approx 2\pi \times 20$ MHz. The sideband cooling can further push the transverse modes to the ground state with $\bar{n}_x \approx 0$ [70–73]. For the axial modes, we only require their thermal motion to be much less than the ion spacing, which is satisfied already under routine Doppler cooling.

As all the local transverse modes have the same frequency (with $t_{i,j} \ll \omega_x$), we only need to apply one step of the sideband cooling independent of the number of ions, with the laser detuning set at $-\omega_x$. The off-resonant process in the sideband cooling limits $\bar{n}_x \sim \gamma/\omega_x$, where γ is the rate of the sideband cooling which needs to be comparable with the phonon hopping rate $t_{i,i+1}$. For a harmonic trap, we take $l_0 = \left[e^2/\left(4\pi\varepsilon_0 m\omega_z^2\right)\right]^{1/3}$ as the length unit so that the ion spacings in this unit take universal dimensionless values (of the order of 1) independent of the ion species and the trap frequency [74].

The hopping rate $t_{i,i+1} \sim t_0/l_0^3 = \omega_z^2/(2\omega_x)$ and the thermal phonon number after the sideband cooling $\bar{n}_x \sim t_{i,i+1}/\omega_x \sim \omega_z^2/\left(2\omega_x^2\right) < 10^{-2}$ with a typical $\omega_z \approx 2\pi \times (0.3 \sim 1)$ MHz. After cooling of all the transverse modes to the ground state, we can then set them to any desired Fock states through a sequence of laser pulses blue detuned at ω_x [75]. Note that the ion spacing is about or larger than 10 μm under our choice of the parameters, and under such a spacing it is reasonable to assume individual addressing of different ions with focused laser beams. The focused beam can

prepare different local modes a_i to different Fock states $|n_i\rangle$. For implementation of the Boson sampling, without loss of generality we actually can choose $n_i = 1$, which requires only one pulse for preparation. To make the phonon hopping negligible during the preparation step, the sideband Rabi frequency Ω needs to be large compared with the hopping rate $t_{i,i+1} \sim \omega_z^2/(2\omega_x) \sim 2\pi \times (10 \sim 100)$ kHz, which is easy to satisfy under typical laser power.

After the state initialization, we need to coherently mix different phonon modes. The inherent Coulomb interaction described by the Hamiltonian (5.3.1) serves this purpose, however, it is constantly on without a tuning knob and we need to introduce additional control parameters to realize different unitary transformations between the M modes. To achieve this goal, we introduce a simple operation which induces a controllable phase shift for any local phonon mode at any desired time. A laser pulse with duration t_p and detuning δ to the sideband induces an additional Hamiltonian $H_i = \hbar\left(\Omega_i^2/\delta\right) a_i^\dagger a_i$ (Ω_i is the sideband Rabi frequency applied to the target ion i), which gives a phase shift $U_{\phi_i} = e^{i\phi_i a_i^\dagger a_i}$ to the mode a_i with $\phi_i = \Omega_i^2 t_p/\delta$. We choose $\Omega_i^2/\delta \gg t_{i,i+1}$ so that the pulse can be considered to be instantaneous over the time scale of phonon tunneling.

The operation U_{ϕ_i} and the Coulomb interaction H_c together are universal in the sense that a combination of them can make any unitary transformation on the M phonon modes represented by the $M \times M$ matrix Λ. Now we prove this statement. It is known that any unitary transformation Λ on M Bosonic modes can be decomposed as a sequence of neighboring beam-splitter-type of operations and individual phase shifts [76]. The beam splitter operation for the modes $(j, j+1)$ is represented by the Hamiltonian $H_{bs}^{(j)} = \hbar t_{j,j+1}\left(a_j a_{j+1}^\dagger + a_{j+1} a_j^\dagger\right)$.

To realize $H_{bs}^{(j)}$, we just need to cut off all the other interaction terms in the Coulomb Hamiltonian given by Eq. (5.3.1) except for a specific pair $(j, j+1)$. This can be achieved through the idea of dynamical decoupling using the fast phase shifts U_{ϕ_i} with $\phi_i = \pi$ [77]. Note that a Hamiltonian term $H_{ij} = \hbar t_{i,j}\left(a_i a_j^\dagger + a_j a_i^\dagger\right)$ can be effectively turned off for an evolution time t if we apply an instantaneous π-phase shift $U_{\phi_i=\pi}$ at time $t/2$ to the mode a_i to flip the sign of H_{ij} to $-H_{ij}$ for the

second half period of the evolution.

The interaction Hamiltonian H_c has long-range tunneling, but it decays fast with distance d through $1/d^3$ scaling. If we take the first order approximation to keep only the nearest neighbor tunneling, the Hamiltonian has the form $H_{NN} = \sum_{i=1}^{M-1} \hbar t_{i,i+1} \left(a_i^\dagger a_{i+1} + a_i a_{i+1}^\dagger \right)$. The Hamiltonian H_{NN} can be used to realize the required coupling $H_{bs}^{(j)}$ for an arbitrary j if we apply π phase shifts at time $t/2$ to every other modes in the ion chain except for the pair $(j, j+1)$ as illustrated in Fig. 5.3.1(a). This kind of decoupling can be extended and we can simulate the Hamiltonian H_{NN} (and thus $H_{bs}^{(j)}$) with the original long range Hamiltonian H_c to an arbitrary order of approximation.

Suppose we cut the interaction range in H_c to the kth order (i.e., we neglect the terms in H_c that scale as $1/d_{ij}^3$ with $|i-j| > k$), we can shrink the interaction range from k to $k-1$ by applying one step of dynamical decoupling with the pattern of π-phase shifts illustrated in Fig. 5.3.1(b). This step can be continued until one reaches H_{NN} through concatenation of the dynamical decoupling [77]. This proves that the Coulomb interaction Hamiltonian H_c, together with the phase shifts U_{ϕ_i} on single ions, can realize any beam splitter operations and thus be universal for construction of arbitrary unitary operations on the M phononic modes.

We should note that the above proof of universality based on the idea of dynamical decoupling is intuitively straight-forward but may be cumbersome to realize in practice. For a real experiment we suggest using optimization methods to design the control sequence for any given unitary. Alternatively, one can randomly generate a sequence of phase shifters and insert them to the evolution to sample unitaries from the group SU(N) randomly (see Appendix C for a demonstration). Due to the universality of the device we are guaranteed to reach almost any corner of the space SU(N). In both approaches, the truncation of Coulomb interaction range is not necessary.

The final step of the Boson sampling is detection of all the phononic modes in the Fock basis. The conventional method of measuring the phonon number distribution of a single mode by recording the spin oscillation from red or blue sideband pulses is not applicable here as it cannot measure cor-

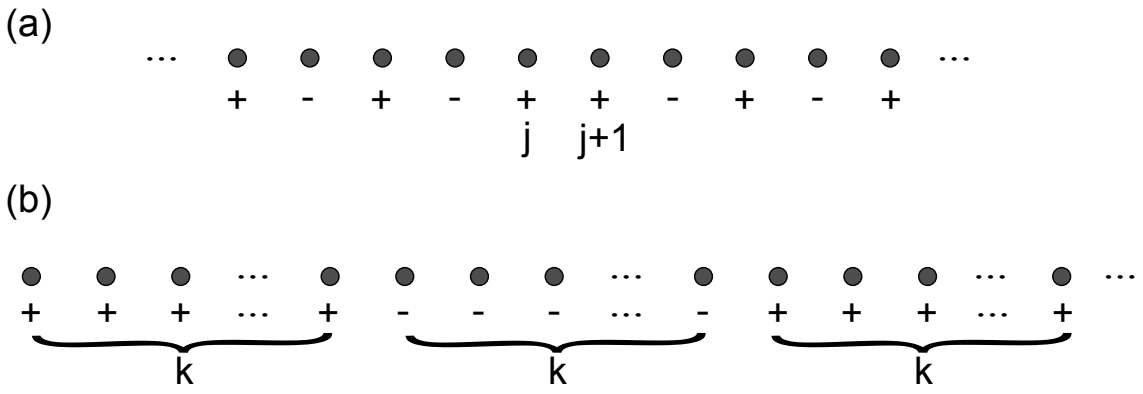

Figure 5.3.1: Control of the tunneling Hamiltonian through the dynamical decoupling. The negative signs in (a,b) denote the set of ions to be applied a π phase shift at half of the evolution time while the positive signs denote the ions left intact. (a) The π-phase pattern to turn off other tunneling terms in H_{NN} except for a neighboring pair $j, j+1$; (b) The π-phase pattern to shrink the tunneling range of the Hamiltonian from k to $k-1$.

relation of different phonon modes in the Fock basis [75]. What we need is a projective measurement of each mode in the Fock basis which gives information of arbitrary high order correlations between different modes.

For trapped ions, a projective measurement of its spin (internal) state can be done with a very high efficiency through the quantum jump technique using a cycling transition. However, the spin detection gives only binary measurement outcomes ("dark" or "bright"). We need to figure out a way to perform projective measurements of the Fock states (with multiple possible outcomes) for each phonon mode through the binary spin detection. This is achieved through a consecutive detection scheme with the following steps:

(1) First, to illustrate the idea, we consider a single ion with its phonon mode in an arbitrary state $\sum_n c_n |n\rangle$ and its spin prepared in the dark state $|D\rangle$ (see Fig. 5.3.2(a)).

(2) Through the well known adiabatic transition technique [78], we make a complete population transfer from $|n+1\rangle|D\rangle$ to $|n\rangle|B\rangle$ for all the Fock components $|n\rangle$ by chirping the frequency of a laser pulse across the red detuning at $-\omega_x$ (see Fig. 5.3.2(b) for the population distribution after

this step).

(3) We make a carrier transition $|n\rangle|D\rangle \rightleftarrows |n\rangle|B\rangle$ with a $\pi-$pulse to flip the dark and the bright states (see Fig. 5.3.2(c)).

(4) After this step, we immediately measure the spin state of the ion through the quantum jump detection. With probability $|c_0|^2$, the outcome is "bright". In this case the measurement is finished and we know the phonon is in the $|n=0\rangle$ state. Otherwise, the spin is in the dark state and the phonon is in the $|n\geq 1\rangle$ components (see Fig. 5.3.2(d) for the population distribution in this case). When the spin is in the dark state, the ion does not scatter any photons during the quantum jump measurement. So its phonon state will not be influenced by this measurement. This feature is important for this consecutive measurement scheme.

(5) Now with the phonons in the $|n\geq 1\rangle$ components, we just repeat the steps (2)-(3)-(4) until finally we get the outcome "bright" for the spin detection. We conclude that the phonon is in the Fock state $|n=l\rangle$ if the outcome "bright" occurs (with probability $|c_l|^2$) after l repetitions of the above steps.

(6) The above consecutive measurement scheme can be extended straightforwardly to measure M local phonon modes in the Fock basis independently with M ions. The only requirement is that the phonon tunneling between different modes is negligible during the measurement process. The slowest step of the measurement is the quantum jump detection of the ion spin state. Recently, there has been experimental report of high efficiency ($> 99\%$) spin state detection within 10 μs detection time [79]. The typical phonon hopping rate between the neighboring ions in our scheme is in the range of $t_{i,i+1} \sim 2\pi \times (10 \sim 100)$ kHz, and this hopping rate can be significantly reduced during the detection through either an expansion of the ion chain along the z direction right before the direction by lowering the axial trap frequency or application of a few dynamical decoupling pulses to turn off the neighboring tunneling during the detection. As the hopping scales as $1/d^3$, a moderate increase of the effective distance d will significantly reduce the tunneling and push it

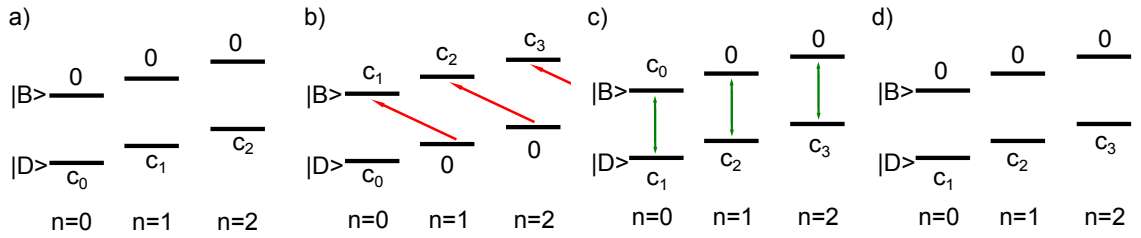

Figure 5.3.2: A consecutive measurement scheme to perform projective detection of the phonon mode in the Fock basis. (a) The initial state configuration right before the measurement. (b-d) The state configuration after the blue sideband transition, the carrier transition, and the quantum jump detection. These three steps are repeated until one finally registers the "bright" state (see the text for details).

below the kHz level. We should note that for the Boson sampling algorithm, the output phonon number per mode is typically small (the conventional photon detectors actually can only distinguish 0 and 1 photons), and the number of repetitions in our consecutive measurement scheme is either zero or very few in most cases.

5.4 Chapter Summary

In summary, we have proposed a scalable scheme to realize the Boson sampling algorithm by use of the local transverse phonon modes of trapped ions. The scheme allows deterministic preparation and high-efficiency readout of the phonon Fock states and universal manipulation of the phonon modes through a combination of inherent Coulomb interaction and individual phase shifts.

Several dozens of ions have been successfully trapped experimentally to form a linear chain, and in principle there is no limitation to the number of ions that can be manipulated in a linear Paul trap by use of anharmonic axial potentials [80]. This scheme thus opens the perspective to realize Boson sampling for dozens of phonons with the state-of-the-art trapped ion technology, which would beat the capability of any classical computers and give the first serious experimental test of the extended Church-Turing thesis.

This chaper contains content that was published elsewhere [81] and is available at

http://link.aps.org/doi/10.1103/PhysRevLett.112.050504.

CHAPTER VII

Conclusions

6.1 Summary

In this dissertation, we have investigated several topics centering around quantum entanglement and quantum information processing with atomic and ionic systems.

In Chapter II we propose a method to generate massive entanglement in a spinor Bose-Einstein condensate from an initial product state through adiabatic sweep of magnetic field across a quantum phase transition induced by competition between the spin-dependent collision interaction and the quadratic Zeeman effect. The generated many-body entanglement is characterized by the experimentally measurable entanglement depth in the proximity of the Dicke state. We show that the scheme is robust to practical noise and experimental imperfection and under realistic conditions it is possible to generate genuine entanglement for hundreds of atoms.

In Chapter III we introduce a new class of quantum many-particle entangled states, called the Dicke squeezed (or DS) states, which can be used to improve the precision in quantum metrology beyond the standard quantum limit. We show that the enhancement in measurement precision is characterized by a single experimentally detectable parameter, called the Dicke squeezing ξ_D, which also

bounds the entanglement depth for this class of states. The measurement precision approaches the ultimate Heisenberg limit as ξ_D attains the minimum in an ideal Dicke state. Compared with other entangled states, we show that the Dicke squeezed states are more robust to decoherence and give better measurement precision under typical experimental noise.

Another states that have strong entanglement and high internal phase precision are the spin squeezed states. They have been proven to be an better platform for precision measurement as these states are easier to prepare in the real experimental condition. A robust squeezing parameter is proposed to characterize the experimental phase measurement precision for spin squeezed states. The behavior of this parameter under various experimental noises is compared with other parameters in the history and it is shown to have better performance.

For the trapped ion platform, we have proposed a scalable scheme to realize the Boson sampling algorithm by use of the local transverse phonon modes of trapped ions. The scheme allows deterministic preparation and high-efficiency readout of the phonon Fock states and universal manipulation of the phonon modes through a combination of inherent Coulomb interaction and individual phase shifts. Several dozens of ions have been successfully trapped experimentally to form a linear chain, and in principle there is no limitation to the number of ions that can be manipulated in a linear Paul trap by use of anharmonic axial potentials [80]. This scheme thus opens the perspective to realize Boson sampling for dozens of phonons with the stateof-the-art trapped ion technology, which would beat the capability of any classical computers and give the first serious experimental test of the extended Church-Turing thesis.

6.2 Outlook

Based on the previous works both presented in this dissertation and in the literature, we now identify several possible directions for future research work in this field.

Dicke state generation methods. The importance of Dicke state in both quantum computation and quantum information processing is tremendous while it is a complicated quantum entangled state that is hard to realise in realistic experiment condition. The coherence time for the system has key impact on the state preparation. Also Dicke states with large number of atoms attract people's interest.

Manybody Entanglement characterization. The entanglement properties for two qubit systems are well described by the von Neumann entropy. However for large number of particles or higher dimentional spin system, there is no universal entanglment measurement parameters. The judgement of the existence of entanglement is not sufficient and entanglement depth parameters with good performance are still needed.

Boson sampling on other platforms. Currently there are two main possible platforms for boson sampling, photons and phonons in ion systems. Other possibilities are also under research. Easy controlling of the particles and scaling feasibility are both factors to be considered.

APPENDICES

APPENDIX A
Spin-1 BEC Hamiltonian Description

The Hamiltonian for the spin-1 condensate can be divided into two parts $H = H_0 + H_i$. The non-interacting Hamiltonian H_0 and the interaction Hamiltonian H_i take respectively the following forms [1, 15]

$$\begin{aligned} \hat{H}_0 &= \sum_{m,n=0,\pm1} \int d\mathbf{r}\, \hat{\psi}_m^\dagger [-\frac{\hbar^2\nabla^2}{2M} \\ &+ U(\mathbf{r}) - p(f_z)_{mn} + q(f_z^2)_{mn}]\hat{\psi}_n, \qquad (6.1.1) \\ \hat{H}_i &= \frac{1}{2}\int d\mathbf{r}[c_0' : \hat{n}^2(\mathbf{r}) : + c_1' : \hat{F}^2(\mathbf{r}) :]. \qquad (6.1.2) \end{aligned}$$

where $\hat{\psi}_m(\mathbf{r})$ denote the bosonic field operators with the spin index $m = 1, 0, -1$, corresponding to annihilation of an atom of mass M in the Zeeman state m on the hyperfine level $F = 1$. The atoms are trapped by the spin-independent optical potential $U(\mathbf{r})$. The linear Zeeman coefficient $p = -g\mu_B B$, where g is the Landé g factor, μ_B is the Bohr magneton, and B is the external magnetic field. The quadratic Zeeman coefficient $q = \frac{(g\mu_B B)^2}{\Delta E_{hf}}$, where ΔE_{hf} is the hyperfine energy splitting. The symbol f_μ ($\mu = x, y, z$) denotes μ-component of the spin-1 matrix, and $(f_\mu)_{mn}$ is the corresponding (m, n) matrix element.

The particle density operator $\hat{n}(\mathbf{r})$ and the spin operator $\hat{F}(\mathbf{r})$ are defined respectively by $\hat{n}(\mathbf{r}) = \sum_{m=-1}^{1} \hat{\psi}_m^\dagger(\mathbf{r})\hat{\psi}_m(\mathbf{r})$ and $\hat{F}_\mu(\mathbf{r}) = \sum_{m,n=-1}^{1}(f_\mu)_{mn}\hat{\psi}_m^\dagger(\mathbf{r})\hat{\psi}_n(\mathbf{r})$. The interaction coefficients $c_0' = 4\pi\hbar^2(a_0 + 2a_2)/3M$, $c_1' = 4\pi\hbar^2(a_2 - a_0)/3M$, where a_s is the s-wave scattering lengths for two

colliding atoms with total spin s. We have $c_1' < 0$ ($c_1' > 0$) for ^{87}Rb (^{23}Na), which corresponds to ferromagnetic (anti-ferromagnetic) interaction, respectively.

For typical spinor condensates in experiments such as ^{87}Rb and ^{23}Na, we have $c_0' \gg c_1'$, so the spin-independent interaction dominates over the spin-dependent interaction. In this case, to describe the ground state in a spin-independent optical trap $U(\mathbf{r})$, it is good approximation to assume that different spin components $\hat{\psi}_m(\mathbf{r})$ of the condensate take the same spatial wave function $\phi(\mathbf{r})$. This is the well-known single mode approximation [1, 17], and under this approximation we have $\hat{\psi}_m \approx \hat{a}_m \phi(\mathbf{r}), (m = 1, 0, -1)$, where a_m is the annihilation operator for corresponding spin mode and $\phi(\mathbf{r})$ is normalized as $\int d\mathbf{r} |\phi(\mathbf{r})|^2 = 1$.

We consider a spinor condensate with a fixed total particle number N as in experiments and neglect the terms in the Hamiltonian that are constant under this condition. The spin-dependent part of the Hamiltonian is then simplified to

$$H = c_1 \frac{\mathbf{L}^2}{N} + \sum_{m=-1}^{1} (qm^2 - pm) a_m^\dagger a_m \tag{6.1.3}$$

as we used in the paper, with $c_1 = c_1' N \int d\mathbf{r} |\phi(\mathbf{r})|^4 / 2$.

APPENDIX B
Calculation of Final State Entanglement Depth

Expanded using the creation and annihilation operators for a spin-i atom $a_i (i = \pm 1, 0)$, Hamiltonian of Eq. 2.3.2 in the main text has the form (with constants neglected)

$H = \frac{c_1}{N}(a_1^\dagger a_1^\dagger a_1 a_1 + a_{-1}^\dagger a_{-1}^\dagger a_{-1} a_{-1} - 2a_1^\dagger a_{-1}^\dagger a_1 a_{-1} + 2a_1^\dagger a_0^\dagger a_0 a_1 + 2a_{-1}^\dagger a_0^\dagger a_0 a_{-1} + 2a_0^\dagger a_0^\dagger a_1 a_{-1} + 2a_1^\dagger a_{-1}^\dagger a_0 a_0) - q a_0^\dagger a_0,$

For computational convenience, we choose the Fock state $|n_1, n_0, n_{-1}\rangle$as the basic state, which is the eigenstate of the number operator $n_i = a_i^\dagger a_i$ for the three spin components. As L_z is conserved in the evolution and considering the particle number conservation, there is only one free parameter with the constraint $n_1 + n_{-1} = 0$ and $n_1 + n_{-1} + n_0 = N$. Thereby the initial state is $|n_0 = N\rangle$.

In our calculation, the quadratic Zeeman coefficient q is ramped with constant speed as $q(t) = (6 - vt)\,|c_1|$(v is the ramping speed of q). The system evolution is governed by the time dependent Schrödinger equation $i\hbar\frac{\partial}{\partial t}\psi = H\psi$. Final state is calculated after unitary evolution and we get the entanglement depth ξ of the final state from Eq. (2.6.1) of main text.

APPENDIX C
Demonstration of Boson Sampling

In this appendix we will perform a classical simulation of the Boson sampling experiment to demonstrate how the proposed scheme works. The hopping Hamiltonian for the local phonons is

$$\begin{aligned} H_{hop} &= \sum_{i<j}^{M} t_{i,j}\left(a_i^\dagger a_j + a_i a_j^\dagger\right) \\ &= \sum_{i,j}^{M} a_i^\dagger H_{ij} a_j. \end{aligned}$$

Combining with the ability to phase shift each oscillator, i.e.

$$a_i \rightarrow a_i \exp(-i\theta_i),$$

we can generate a series of Hamiltonians

$$H_{hop}(\vec{\theta}) = \sum_{i,j}^{M} a_i^\dagger H_{ij} a_j \exp\left(i(\theta_i - \theta_j)\right).$$

By tuning the $\vec{\theta}$ vector we have the freedom to engineer the effective Hamiltonian. In addition we are also free to choose the evolution time t for a particular choice of $\vec{\theta}$. So our building block of

the evolution is

$$\begin{aligned} U(\vec{\theta},t) &= \exp\left(-iH_{hop}(\vec{\theta})t\right) \\ &= \exp\left(-i\sum_{i,j}^{M} a_i^{\dagger} H_{ij} \exp\left(i(\theta_i-\theta_j)\right) a_j\right) \end{aligned}$$

Noting that the Hamlitonians $H_{hop}(\vec{\theta})$ are quadratic in a and $a^{\dagger}$, a canonical transformation can be performed to find the normal modes b_i satisfying $b_i = u_{ij}a_j$ so that

$$U(\vec{\theta},t) = \exp\left(-i\sum_j D_{jj} b_j^{\dagger} b_j\right)$$

where D is a diagonal matrix resulting from the canonical transformation. This evolution operator is nothing more than a set of phase shifters for the phonon modes b_j, each of which having a phase shift D_{jj}. Therefore the overall effect of $U(\vec{\theta},t)$ can be described as a three-step process: (1) do a basis transformation from a_i to b_j; (2) phase shift each mode b_j; (3) transform back to the original basis. Thus the output of $U(\vec{\theta},t)$ can be related to the input as

$$\begin{aligned} \vec{a}' &= u^{\dagger} diag(e^{-iD_{11}}, e^{-iD_{22}}, \cdots) u\vec{a} \\ &= \Lambda(\vec{\theta},t)\vec{a}. \end{aligned}$$

The universality of the model was established in the main text of Chapter II, so one can concatenate the building blocks $\Lambda(\theta,t)$ to form an arbitrary N-dimensional unitary in principle. Notice that the computation of $\Lambda(\theta,t)$ given parameters$\vec{\theta}$ and t only requires diagonalizing an $N \times N$ matrix so it can be done very efficiently.

Now let us work out a numerical example and study the effect of control noise in the $\vec{\theta}$ vectors. We assume $N = 10$ ions, calculated the equilibrium positions in a trap with aspect ratio $\omega_x/\omega_z = 10$, and found the hopping coefficients $t_{ij} = t_0/\left|z_i^0 - z_j^0\right|^3$. We consider a three stage evolution

$U_3 = \prod_{i=1}^{3} U(\vec{\theta}_i, t)$ with randomly chosen $\vec{\theta}_i$ and fixed $t = 1/t_0$. Following the approach above, the corresponding $\Lambda_3 = \prod_{i=1}^{3} \Lambda(\vec{\theta}_i, t)$ can be easily found. Then we introduce Gaussian random additive errors to all the $\vec{\theta}_i$ with zero mean and standard deviation σ. For different values of σ we calculate the distance between $\Lambda_3^{'}$ with noise and the ideal Λ_3. To remove the irrelevant local phase factors for each mode, we define a distance measure as follows

$$dist(\Lambda, \Lambda^{'}) \equiv 1 - \frac{1}{N} \sum_{j=1}^{N} \left| \sum_{i=1}^{N} \Lambda_{ij}^{*} \Lambda_{ij}^{'} \right| .$$

This distance measure essentially is determined by the average absolute value of the inner products of corresponding column vectors from the two unitaries. Only when each column of Λ and $\Lambda^{'}$ is the same up to a phase factor, the distance is zero. We plot the distance from the ideal unitary as a function of σ in Fig. B.1. We can see from the figure that Λ_3 is quite robust against random noise in the parameters $\vec{\theta}_i$.

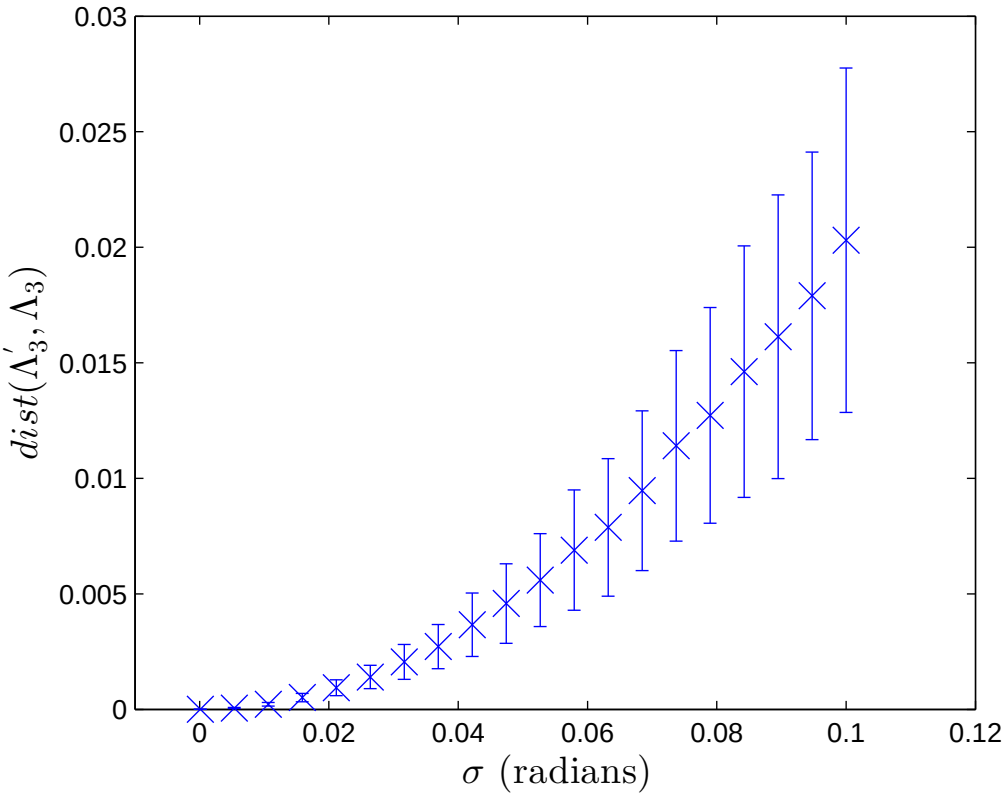

Figure B.1: Distance between the transformation with error $\Lambda_3^{'}$ and the ideal transformation Λ_3, as a function of the standard deviation of the noise σ. Each data point is obtained with 1000 randomized simulation of the noise for a fixed set of arbitrary $\vec{\theta}_i$. The error bar is show one standard deviation of the quantity. See text for detailed parameters used for the system.

BIBLIOGRAPHY

BIBLIOGRAPHY

[1] Dan M. Stamper-Kurn and Masahito Ueda. Spinor bose gases: Symmetries, magnetism, and quantum dynamics. *Rev. Mod. Phys.*, 85:1191–1244, Jul 2013.

[2] Norman F. Ramsey. A molecular beam resonance method with separated oscillating fields. *Phys. Rev.*, 78:695–699, Jun 1950.

[3] F. Bloch. Nuclear induction. *Phys. Rev.*, 70:460–474, Oct 1946.

[4] N Shiga and M Takeuchi. Locking the local oscillator phase to the atomic phase via weak measurement. *New Journal of Physics*, 14(2):023034, 2012.

[5] W. M. Itano, J. C. Bergquist, J. J. Bollinger, J. M. Gilligan, D. J. Heinzen, F. L. Moore, M. G. Raizen, and D. J. Wineland. Quantum projection noise: Population fluctuations in two-level systems. *Phys. Rev. A*, 47:3554–3570, May 1993.

[6] J. J . Bollinger, Wayne M. Itano, D. J. Wineland, and D. J. Heinzen. Optimal frequency measurements with maximally correlated states. *Phys. Rev. A*, 54:R4649–R4652, Dec 1996.

[7] D. J. Wineland, J. J. Bollinger, W. M. Itano, and D. J. Heinzen. Squeezed atomic states and projection noise in spectroscopy. *Phys. Rev. A*, 50:67–88, Jul 1994.

[8] Masahiro Kitagawa and Masahito Ueda. Squeezed spin states. *Phys. Rev. A*, 47:5138–5143, Jun 1993.

[9] C. Gross, T. Zibold, E. Nicklas, J. Estève, and M. K. Oberthaler. Nonlinear atom interferometer surpasses classical precision limit. *Nature*, 464(7292):1165–1169, April 2010.

[10] Max F. Riedel, Pascal BÃ¶hi, Yun Li, Theodor W. Hänsch, Alice Sinatra, and Philipp Treutlein. Atom-chip-based generation of entanglement for quantum metrology. *Nature*, 464(7292):1170–1173, April 2010.

[11] C. Shen and L.-M. Duan. Efficient spin squeezing with optimized pulse sequences. *Phys. Rev. A*, 87:051801, May 2013.

[12] J. I. Cirac and P. Zoller. Quantum computations with cold trapped ions. *Physical Review Letters*, 74(20):4091–4094, May 1995.

[13] Ferdinand Schmidt-Kaler, Hartmut Häffner, Mark Riebe, Stephan Gulde, Gavin P. T. Lancaster, Thomas Deuschle, Christoph Becher, Christian F. Roos, Jürgen Eschner, and Rainer Blatt. Realization of the Cirac-Zoller controlled-NOT quantum gate. *Nature*, 422(6930):408–411, March 2003.

[14] Thomas Monz, Philipp Schindler, Julio T. Barreiro, Michael Chwalla, Daniel Nigg, William A. Coish, Maximilian Harlander, Wolfgang Hänsel, Markus Hennrich, and Rainer Blatt. 14-Qubit Entanglement: Creation and Coherence. *Physical Review Letters*, 106(13):130506, March 2011.

[15] Tin-Lun Ho. Spinor Bose Condensates in Optical Traps. *Physical Review Letters*, 81(4):742–745, July 1998.

[16] Tetsuo Ohmi and Kazushige Machida. Bose-Einstein Condensation with Internal Degrees of Freedom in Alkali Atom Gases. *Journal of the Physical Society of Japan*, 67(6):1822–1825, June 1998.

[17] C. K. Law, H. Pu, and N. P. Bigelow. Quantum Spins Mixing in Spinor Bose-Einstein Condensates. *Physical Review Letters*, 81(24):5257–5261, December 1998.

[18] A. Sorensen, L.-M. Duan, J. I. Cirac, and P. Zoller. Many-particle entanglement with Bose-Einstein condensates. *Nature*, 409(6816):63–66, January 2001.

[19] L.-M. Duan, J. I. Cirac, and P. Zoller. Quantum entanglement in spinor Bose-Einstein condensates. *Physical Review A*, 65(3):033619, February 2002.

[20] C. D. Hamley, C. S. Gerving, T. M. Hoang, E. M. Bookjans, and M. S. Chapman. Spin-nematic squeezed vacuum in a quantum gas. *Nature Physics*, 8(4):305–308, April 2012.

[21] Anders S. Sorensen and Klaus Molmer. Entanglement and Extreme Spin Squeezing. *Physical Review Letters*, 86(20):4431–4434, May 2001.

[22] Ming-Shien Chang, Qishu Qin, Wenxian Zhang, Li You, and Michael S. Chapman. Coherent spinor dynamics in a spin-1 BoseÂ condensate. *Nature Physics*, 1(2):111–116, November 2005.

[23] Y. Liu, S. Jung, S. E. Maxwell, L. D. Turner, E. Tiesinga, and P. D. Lett. Quantum Phase Transitions and Continuous Observation of Spinor Dynamics in an Antiferromagnetic Condensate. *Physical Review Letters*, 102(12):125301, March 2009.

[24] M. J. Holland and K. Burnett. Interferometric detection of optical phase shifts at the Heisenberg limit. *Physical Review Letters*, 71(9):1355–1358, August 1993.

[25] John K. Stockton, J. M. Geremia, Andrew C. Doherty, and Hideo Mabuchi. Characterizing the entanglement of symmetric many-particle spin-$\frac{1}{2}$ systems. *Physical Review A*, 67(2):022112, February 2003.

[26] W. Dür, G. Vidal, and J. I. Cirac. Three qubits can be entangled in two inequivalent ways. *Physical Review A*, 62(6):062314, November 2000.

[27] K. S. Choi, A. Goban, S. B. Papp, S. J. van Enk, and H. J. Kimble. Entanglement of spin waves among four quantum memories. *Nature*, 468(7322):412–416, November 2010.

[28] Witlef Wieczorek, Roland Krischek, Nikolai Kiesel, Patrick Michelberger, Géza Tóth, and Harald Weinfurter. Experimental Entanglement of a Six-Photon Symmetric Dicke State. *Physical Review Letters*, 103(2):020504, July 2009.

[29] A. Acín, D. Brub, M. Lewenstein, and A. Sanpera. Classification of Mixed Three-Qubit States. *Physical Review Letters*, 87(4):040401, July 2001.

[30] L.-M. Duan. Entanglement Detection in the Vicinity of Arbitrary Dicke States. *Physical Review Letters*, 107(18):180502, October 2011.

[31] Fabrice Gerbier, Artur Widera, Simon Fölling, Olaf Mandel, and Immanuel Bloch. Resonant control of spin dynamics in ultracold quantum gases by microwave dressing. *Physical Review A*, 73(4):041602, April 2006.

[32] E. M. Bookjans, A. Vinit, and C. Raman. Quantum Phase Transition in an Antiferromagnetic Spinor Bose-Einstein Condensate. *Physical Review Letters*, 107(19):195306, November 2011.

[33] C. Shen and L.-M. Duan. Correcting detection errors in quantum state engineering through data processing. *New Journal of Physics*, 14(5):053053, May 2012.

[34] Z. Zhang and L.-M. Duan. Generation of Massive Entanglement through an Adiabatic Quantum Phase Transition in a Spinor Condensate. *Physical Review Letters*, 111(18):180401, October 2013.

[35] Vittorio Giovannetti, Seth Lloyd, and Lorenzo Maccone. Quantum-Enhanced Measurements: Beating the Standard Quantum Limit. *Science*, 306(5700):1330–1336, November 2004.

[36] Bernard Yurke, Samuel L. McCall, and John R. Klauder. SU(2) and SU(1,1) interferometers. *Physical Review A*, 33(6):4033–4054, June 1986.

[37] D. J. Wineland, J. J. Bollinger, W. M. Itano, F. L. Moore, and D. J. Heinzen. Spin squeezing and reduced quantum noise in spectroscopy. *Physical Review A*, 46(11):R6797–R6800, December 1992.

[38] D. J. Wineland, J. J. Bollinger, W. M. Itano, and D. J. Heinzen. Squeezed atomic states and projection noise in spectroscopy. *Physical Review A*, 50(1):67–88, July 1994.

[39] J. J . Bollinger, Wayne M. Itano, D. J. Wineland, and D. J. Heinzen. Optimal frequency measurements with maximally correlated states. *Physical Review A*, 54(6):R4649–R4652, December 1996.

[40] E. M. Kessler, P. Kómár, M. Bishof, L. Jiang, A. S. Sørensen, J. Ye, and M. D. Lukin. Heisenberg-limited atom clocks based on entangled qubits. *Phys. Rev. Lett.*, 112:190403, May 2014.

[41] Pieter Kok, Hwang Lee, and Jonathan P. Dowling. Creation of large-photon-number path entanglement conditioned on photodetection. *Physical Review A*, 65(5):052104, April 2002.

[42] Agedi N. Boto, Pieter Kok, Daniel S. Abrams, Samuel L. Braunstein, Colin P. Williams, and Jonathan P. Dowling. Quantum interferometric optical lithography: Exploiting entanglement to beat the diffraction limit. *Phys. Rev. Lett.*, 85:2733–2736, Sep 2000.

[43] D. Leibfried, M. D. Barrett, T. Schaetz, J. Britton, J. Chiaverini, W. M. Itano, J. D. Jost, C. Langer, and D. J. Wineland. Toward Heisenberg-Limited Spectroscopy with Multiparticle Entangled States. *Science*, 304(5676):1476–1478, June 2004.

[44] J. Appel, P. J. Windpassinger, D. Oblak, U. B. Hoff, N. Kjargaard, and E. S. Polzik. Mesoscopic atomic entanglement for precision measurements beyond the standard quantum limit. *Proceedings of the National Academy of Sciences*, 106(27):10960–10965, July 2009.

[45] Anne Louchet-Chauvet, Jürgen Appel, Jelmer J. Renema, Daniel Oblak, Niels Kjaergaard, and Eugene S. Polzik. Entanglement-assisted atomic clock beyond the projection noise limit. *New Journal of Physics*, 12(6):065032, June 2010.

[46] Ian D. Leroux, Monika H. Schleier-Smith, and Vladan Vuletić. Implementation of Cavity Squeezing of a Collective Atomic Spin. *Physical Review Letters*, 104(7):073602, February 2010.

[47] Shi-Liang Zhu, C. Monroe, and L.-M. Duan. Trapped ion quantum computation with transverse phonon modes. *Physical Review Letters*, 97(5):050505, August 2006.

[48] D. Meiser and M. J. Holland. Robustness of Heisenberg-limited interferometry with balanced Fock states. *New Journal of Physics*, 11(3):033002, March 2009.

[49] S. F. Huelga, C. Macchiavello, T. Pellizzari, A. K. Ekert, M. B. Plenio, and J. I. Cirac. Improvement of Frequency Standards with Quantum Entanglement. *Physical Review Letters*, 79(20):3865–3868, November 1997.

[50] Taesoo Kim, Olivier Pfister, Murray J. Holland, Jaewoo Noh, and John L. Hall. Influence of decorrelation on Heisenberg-limited interferometry with quantum correlated photons. *Physical Review A*, 57(5):4004–4013, May 1998.

[51] Giuseppe Vitagliano, Iagoba Apellaniz, Iñigo L. Egusquiza, and Géza Tóth. Spin squeezing and entanglement for an arbitrary spin. *Physical Review A*, 89(3):032307, March 2014.

[52] D. T. Pegg and S. M. Barnett. Phase properties of the quantized single-mode electromagnetic field. *Physical Review A*, 39(4):1665–1675, February 1989.

[53] Rafał Demkowicz-Dobrzański, Jan Kołodyński, and Mădălin Guţă. The elusive Heisenberg limit in quantum-enhanced metrology. *Nature Communications*, 3:1063, September 2012.

[54] Bernd Lücke, Jan Peise, Giuseppe Vitagliano, Jan Arlt, Luis Santos, Géza Tóth, and Carsten Klempt. Detecting Multiparticle Entanglement of Dicke States. *Physical Review Letters*, 112(15):155304, April 2014.

[55] Z Zhang and L M Duan. Quantum metrology with dicke squeezed states. *New Journal of Physics*, 16(10):103037, 2014.

[56] Xiao-Qi Zhou, Hugo Cable, Rebecca Whittaker, Peter Shadbolt, Jeremy L. O'Brien, and Jonathan C. F. Matthews. Quantum-enhanced tomography of unitary processes. *arXiv:1402.2897 [quant-ph]*, February 2014. arXiv: 1402.2897.

[57] P. Bouyer and M. A. Kasevich. Heisenberg-limited spectroscopy with degenerate bose-einstein gases. *Phys. Rev. A*, 56:R1083–R1086, Aug 1997.

[58] Scott Aaronson and Alex Arkhipov. The computational complexity of linear optics. In *Proceedings of the Forty-third Annual ACM Symposium on Theory of Computing*, STOC '11, pages 333–342, New York, NY, USA, 2011. ACM.

[59] Peter W. Shor. Polynomial-time algorithms for prime factorization and discrete logarithms on a quantum computer. *SIAM Journal on Computing*, 26(5):1484–1509, October 1997.

[60] L. G. Valiant. The complexity of computing the permanent. *Theoretical Computer Science*, 8(2):189–201, 1979.

[61] Justin B. Spring, Benjamin J. Metcalf, Peter C. Humphreys, W. Steven Kolthammer, Xian-Min Jin, Marco Barbieri, Animesh Datta, Nicholas Thomas-Peter, Nathan K. Langford, Dmytro Kundys, James C. Gates, Brian J. Smith, Peter G. R. Smith, and Ian A. Walmsley. Boson sampling on a photonic chip. *Science*, 339(6121):798–801, February 2013.

[62] Matthew A. Broome, Alessandro Fedrizzi, Saleh Rahimi-Keshari, Justin Dove, Scott Aaronson, Timothy C. Ralph, and Andrew G. White. Photonic boson sampling in a tunable circuit. *Science*, 339(6121):794–798, February 2013.

[63] Max Tillmann, Borivoje Dakic, Rene Heilmann, Stefan Nolte, Alexander Szameit, and Philip Walther. Experimental boson sampling. *Nature Photonics*, 7(7):540–544, July 2013.

[64] Andrea Crespi, Roberto Osellame, Roberta Ramponi, Daniel J. Brod, Ernesto F. Galvao, Nicolo Spagnolo, Chiara Vitelli, Enrico Maiorino, Paolo Mataloni, and Fabio Sciarrino. Integrated multimode interferometers with arbitrary designs for photonic boson sampling. *Nature Photonics*, 7(7):545–549, July 2013.

[65] C. Gogolin, M. Kliesch, L. Aolita, and J. Eisert. Boson-sampling in the light of sample complexity. *arXiv:1306.3995 [quant-ph]*, June 2013.

[66] Scott Aaronson and Alex Arkhipov. BosonSampling is far from uniform. *arXiv:1309.7460 [quant-ph]*, September 2013.

[67] Stefan Scheel. Permanents in linear optical networks. *arXiv:quant-ph/0406127*, June 2004.

[68] D. Porras and J. I. Cirac. Bose-Einstein condensation and strong-correlation behavior of phonons in ion traps. *Physical Review Letters*, 93(26):263602, December 2004.

[69] X.-L. Deng, D. Porras, and J. I. Cirac. Quantum phases of interacting phonons in ion traps. *Physical Review A*, 77(3):033403, March 2008.

[70] F. Diedrich, J. C. Bergquist, Wayne M. Itano, and D. J. Wineland. Laser cooling to the zero-point energy of motion. *Physical Review Letters*, 62(4):403–406, January 1989.

[71] C. Monroe, D. M. Meekhof, B. E. King, S. R. Jefferts, W. M. Itano, D. J. Wineland, and P. Gould. Resolved-sideband raman cooling of a bound atom to the 3D zero-point energy. *Physical Review Letters*, 75(22):4011–4014, November 1995.

[72] B. E. King, C. S. Wood, C. J. Myatt, Q. A. Turchette, D. Leibfried, W. M. Itano, C. Monroe, and D. J. Wineland. Cooling the collective motion of trapped ions to initialize a quantum register. *Physical Review Letters*, 81(7):1525–1528, August 1998.

[73] G. Poulsen, Y. Miroshnychenko, and M. Drewsen. Efficient ground-state cooling of an ion in a large room-temperature linear paul trap with a sub-hertz heating rate. *Physical Review A*, 86(5):051402, November 2012.

[74] D. F. V. James. Quantum dynamics of cold trapped ions with application to quantum computation. *Applied Physics B*, 66(2):181–190, February 1998.

[75] D. M. Meekhof, C. Monroe, B. E. King, W. M. Itano, and D. J. Wineland. Generation of nonclassical motional states of a trapped atom. *Physical Review Letters*, 76(11):1796–1799, March 1996.

[76] Michael Reck, Anton Zeilinger, Herbert J. Bernstein, and Philip Bertani. Experimental realization of any discrete unitary operator. *Physical Review Letters*, 73(1):58–61, July 1994.

[77] Hui Khoon Ng, Daniel A. Lidar, and John Preskill. Combining dynamical decoupling with fault-tolerant quantum computation. *Physical Review A*, 84(1):012305, July 2011.

[78] T. Watanabe, S. Nomura, K. Toyoda, and S. Urabe. Sideband excitation of trapped ions by rapid adiabatic passage for manipulation of motional states. *Physical Review A*, 84(3):033412, September 2011.

[79] Rachel Noek, Geert Vrijsen, Daniel Gaultney, Emily Mount, Taehyun Kim, Peter Maunz, and Jungsang Kim. High speed, high fidelity detection of an atomic hyperfine qubit. *arXiv:1304.3511 [quant-ph]*, April 2013.

[80] G.-D. Lin, S.-L. Zhu, R. Islam, K. Kim, M.-S. Chang, S. Korenblit, C. Monroe, and L.-M. Duan. Large-scale quantum computation in an anharmonic linear ion trap. *EPL (Europhysics Letters)*, 86(6):60004, June 2009.

[81] C. Shen, Z. Zhang, and L.-M. Duan. Scalable implementation of boson sampling with trapped ions. *Phys. Rev. Lett.*, 112:050504, Feb 2014.

[82] Anders S. Sørensen and Klaus Mølmer. Entanglement and extreme spin squeezing. *Phys. Rev. Lett.*, 86:4431–4434, May 2001.

[83] A. André, A. S. Sørensen, and M. D. Lukin. Stability of atomic clocks based on entangled atoms. *Phys. Rev. Lett.*, 92:230801, Jun 2004.

[84] R. P. Feynman. Simulating physics with computers. *International Journal of Theoretical Physics*, 21:467–488, June 1982.

[85] R. Blatt and C. F. Roos. Quantum simulations with trapped ions. *Nature Physics*, 8(4):277–284, April 2012.

[86] Anders Sørensen and Klaus Mølmer. Quantum computation with ions in thermal motion. *Physical Review Letters*, 82(9):1971–1974, March 1999.

[87] B. E. King. *Quantum State Engineering and Information Processing with Trapped Ions*. PhD thesis, University of Colorado at Boulder, 1999.

[88] D. Deutsch. Quantum theory, the church-turing principle and the universal quantum computer. In *Proceedings of the Royal Society of London*, volume 400 of *A. Mathematical and Physical Sciences*, pages 97–117, July 1985.

[89] D. Deutsch and R. Jozsa. Rapid solutions of problems by quantum computation. In *Proceedings of the Royal Society of London*, volume 439, page 553, 1985.

[90] C. H. Bennet and G. Brassard. Quantum cryptography: Public key distribution and coin tossing. In *Proceedings of the IEEE International Conference on Computers, Systems, and Signal Processing*, page 175, 1984.

[91] Hoi-Kwan Lau and Daniel F. V. James. Proposal for a scalable universal bosonic simulator using individually trapped ions. *Physical Review A*, 85(6):062329, June 2012.

[92] H. Häffner, W. Hänsel, C. F. Roos, J. Benhelm, D. Chek-al kar, M. Chwalla, T. Körber, U. D. Rapol, M. Riebe, P. O. Schmidt, C. Becher, O. GÃŒhne, W. Dür, and R. Blatt. Scalable multiparticle entanglement of trapped ions. *Nature*, 438(7068):643–646, December 2005.